Renormalization of stochastic lattice models: Basic formulation

Christoph A. Haselwandter* and Dimitri D. Vvedensky
The Blackett Laboratory, Imperial College London, London SW7 2AZ, United Kingdom
(Received 11 June 2007; published 8 October 2007)

We describe a general method for the multiscale analysis of stochastic lattice models. Beginning with a lattice Langevin formulation of site fluctuations, we derive stochastic partial differential equations by regularizing the transition rules of the model. Subsequent coarse graining is accomplished by calculating renormalization-group (RG) trajectories from initial conditions determined by the regularized atomistic models. The RG trajectories correspond to hierarchies of continuum equations describing lattice models over expanding length and time scales. These continuum equations retain a quantitative connection over different scales, as well as to the underlying atomistic dynamics. This provides a systematic method for the derivation of continuum equations from the transition rules of lattice models for any length and time scales. As an illustration we consider the one-dimensional (1D) Wolf-Villain (WV) model [Europhys. Lett. **13**, 389 (1990)]. The RG analysis of this model, which we develop in detail, is generic and can be applied to a wide range of conservative lattice models. The RG trajectory of the 1D WV model shows a complex crossover sequence of linear and nonlinear stochastic differential equations, which is in excellent agreement with kinetic Monte Carlo simulations of this model. We conclude by discussing possible applications of the multiscale method described here to other nonequilibrium systems.

DOI: 10.1103/PhysRevE.76.041115 PACS number(s): 05.40.−a, 81.15.Aa, 05.10.Gg

I. INTRODUCTION

Nonequilibrium systems are characterized by the presence of a driving force which prevents global equilibration through thermodynamics and renders the state of the system metastable or even unstable. The behavior of such systems is often determined by fluctuations [1–5] that can carry the system into different metastable states. An important source of noise are fluctuations in the driving force itself, such as the shot noise in the particle deposition flux during surface growth. Randomness can also be an inherent property of the medium through which the system is driven, as in the case of fluid flow through a porous material.

The theoretical description of critical or self-organized nonequilibrium systems presents an especially acute challenge due to the interplay between many length and time scales [6]. In particular, fluctuations at atomistic scales can have a profound effect on the macroscopic properties of the system, in which case one must absorb atomistic degrees of freedom into macroscopic variables. A common starting point [1–9] for theoretical studies is the representation of nonequilibrium phenomena by discrete dynamical systems whose behavior is completely specified by relatively simple updating rules. Such *lattice models* appear in various guises throughout science and, depending on the context, are also referred to as *lattice gases* or *cellular automata*. The transition rules of such models are designed to capture the essence of atomic-scale interactions and can involve deterministic and stochastic components.

Lattice models have been used as an alternative to continuum models of nonequilibrium systems whereby the transition rules represent a hugely simplified form of the atomistic dynamics that produces a given macroscopic behavior. Classic implementations of this approach can be found in the field of fluid dynamics [4,5,10], where it has been shown that, in some appropriate limits, cellular automaton models can represent the Navier-Stokes equations. With this approach the rules of lattice models are formulated with a particular continuum theory in mind and do not necessarily represent the actual atomistic processes in the system. Indeed, these rules need not have any physical significance at all [5].

On the other hand, lattice models are also employed as simplified descriptions of the "true" atomistic dynamics in a system [6]. As an example of this approach, consider the epitaxial growth of crystalline surfaces [11–16]. With modern computational capabilities it is possible to determine the dominant atomistic processes for a given materials system and experimental setup using only first-principles methods [17,18]. The resulting catalog of transition rates then defines a lattice model [6,19] that includes the most important atomistic processes. Less important processes have slower transition rates and can therefore be eliminated in a systematic manner. Taking a more empirical approach, lattice models for epitaxial growth can also be formulated from basic physical considerations. The values of the parameters in such models are then obtained through direct comparisons with experiments [20,21].

Given a lattice model for a particular experimental scenario, the most straightforward way to proceed is to perform computer simulations using these transition rules. On this basis lattice models have been used to great effect for the modeling of nonequilibrium phenomena. But lattice models can also serve as the starting point for a theoretical analysis of nonequilibrium systems. As an illustration, let us return to the example of surface growth. The formulation of lattice models for the dominant atomistic processes on surfaces represents an enormous simplification of the equations of quantum mechanics operating at such scales. The question therefore arises quite naturally whether the description of the

*Present address: Department of Physics, Massachusetts Institute of Technology, Cambridge, MA 02139, USA.

system can be reduced further to only its most basic components. It is found that this can indeed be achieved through the formulation of *asymptotic* continuum equations [1,2] based on symmetry considerations and conservation laws. A prominent example of such an equation is the Kardar-Parisi-Zhang equation [22] governing nonconserved surface growth. Each asymptotic continuum equation defines a universality class, which provides the ultimate reduction of lattice models to their most basic components.

Part of the appeal of continuum equations is that they provide a unified description for a large class of lattice models. This, however, also makes a detailed investigation of stochastic lattice models in terms of such continuum equations all but impossible, which severely restricts their predictive power. As an illustration of this problem, consider the case of homoepitaxial surface growth, in which substrate and deposit are the same material. It is found that the standard equations put forward for this scenario [22–31] fail to predict the surface morphologies observed in recent experiments [32–36] and simulations of lattice models [37–39]. Moreover, the absence of a direct relation between the terms in the continuum equations postulated for homoepitaxial growth and any underlying atomistic process means that the coefficients in these continuum equations are in effect arbitrary, which makes quantitative comparisons with experiments difficult [34–36]. Thus, even basic features of experimentally observed homoepitaxial morphologies, such as whether or not the underlying growth dynamics conserve the particle number, remain controversial in some situations [34,35,40,41].

To establish a direct connection with atomistic processes, it is necessary to systematically *derive* continuum equations from stochastic lattice models. A formal procedure for accomplishing this was first proposed in Ref. [42]. Subsequently, similar ideas were used to obtain continuum equations for a variety of growth models (see, e.g., Refs. [43,44]). The continuum equations obtained with this methodology represent a description of lattice models only in the sense that they capture the asymptotic universality class (the "hydrodynamic limit") of these models. The regularization used to transform the master equation to a stochastic partial differential equation was purely formal, in that the magnitudes and signs of the coefficients had no direct relation to the underlying atomistic processes and there was no notion of convergence in this expansion. Thus, finite-order equations consistent with the symmetry of the underlying atomistic processes were obtained from an *ad hoc* truncation of an infinite series of successively higher-order derivatives. The asymptotic universality classes of the atomistic models were then deduced on the basis of renormalization-group (RG) arguments.

The purpose of this paper is to provide a detailed discussion of a method [45,46] for systematically deriving continuum equations that retain a quantitative connection to the transition rules of lattice models for all length and time scales. Our basic strategy is to renormalize regularized continuum representations of stochastic lattice models. This provides a natural method for the reduction of lattice models to their essential components that are appropriate for particular length and time scales. The outcome of this procedure is a hierarchy of continuum equations describing a given lattice model over expanding length and time scales. For each scale, the coefficients in these equations take specific numerical values that are determined by the renormalized parameters appearing in the underlying stochastic lattice model. Coupled with the aforementioned determination of the transition processes and rates through first-principles methods, this offers the promise of a genuine multiscale atomic-to-continuum description of fluctuating nonequilibrium systems.

The main methodological advances discussed in this paper are (i) a systematic regularization of stochastic lattice models that yields continuum equations with the correct form *and* with coefficients whose signs and magnitudes are appropriate for the lattice transition rules at microscopic scales; (ii) with these regularized equations as initial conditions, RG trajectories are calculated that describe lattice models for all transient regimes, which are of primary experimental interest [34–36], prior to the crossover to the asymptotically stable fixed point. Thus, our key result is that the procedure presented here yields hierarchies of continuum equations describing lattice models over any scales, rather than only the asymptotic equations found with the aforementioned approaches. Apart from shorter communications on this work by the present authors [45,46], this is the first time that RG trajectories have been calculated from the rules of atomistic growth models. The focus of this paper is on general aspects of our method. The application of these ideas to lattice models of epitaxial growth on two-dimensional substrates is described in greater detail in a companion publication [47].

The organization of this paper is as follows. In Secs. II and III we outline our approach to the multiscale analysis of stochastic lattice models. Section II summarizes the derivation [42,48–50] of Langevin equations from the Chapman-Kolmogorov equation defining the dynamics of Markovian lattice models. These Langevin equations embody the full transition rules of lattice models, but are simple enough to allow a direct mathematical analysis. As explained in Sec. III, the regularized versions of these Langevin equations provide initial conditions for RG transformations. Each point along the RG trajectory corresponds to the equation of motion appropriate for a given system at that scale whose (renormalized) coefficients are determined by the underlying lattice model. The universal equation for the system is associated with the asymptotically stable fixed point approached by the RG trajectory. This provides a systematic justification of the description of stochastic lattice models by continuum equations for any scale.

In Sec. IV we illustrate our multiscale method for the Wolf-Villain (WV) model [51,52]. Kinetic Monte Carlo (KMC) simulations of the WV model [49,51–54] suggest a complex crossover sequence of linear and nonlinear continuum equations, which provides a critical test for our approach. The RG analysis of the WV model, which is discussed in general terms in Sec. III and in greater detail in Appendix A, is generic and can be applied to a wide range of conservative growth models. Section V contains a discussion of the application of our method to other types of stochastic lattice models. A summary and conclusions are provided in Sec. VI.

II. ATOMISTIC LANGEVIN EQUATIONS

The starting point for our multiscale theory is the regularized description of lattice models in the form of stochastic partial differential equations, which provide the initial conditions for a subsequent RG analysis. The derivation of these equations is achieved in two basic steps. The transition rules of lattice models are first expressed as Langevin equations for the particle fluctuations at each lattice site. The details of this procedure are described in Ref. [49] and summarized in Sec. II A. The second step is the regularization of these Langevin equations. For many lattice models, particularly lattice models describing the morphological evolution of surfaces during growth, which are our main focus here, the transition rules have a threshold character. This arises quite naturally when these rules are expressed in terms of characteristics of the local environments of particles, such as heights or the number of nearest neighbors. The key element of this step is the regularization of the threshold functions in a manner that respects the rules of the original model. This is discussed in Sec. II B. All of the calculations described here are for one-dimensional (1D) systems, but the formalism can be adapted to any lattice dimension. A future publication [47] will describe the application of our methodology to two-dimensional systems.

A. Lattice Langevin equations

We consider lattice models that are completely characterized by a "height" array $\mathbf{H}_n \equiv \{H_1, H_2, \ldots, H_L\}$ at each discrete time step t_n for a lattice of size L. The height at each lattice site denotes the number of particles at that site and, depending on the model, can also be viewed as the particle density. The transition rates of such models described by $\mathbf{H}_n$ depend only on the instantaneous height profile, not on its history. Lattice models that satisfy this condition are referred to as "Markovian" and are used to model a great variety of physical phenomena [1–5,55]. The statistical properties of Markovian lattice models are embodied by the Chapman-Kolmogorov equation [55] for the transition probability $T_{t+t'}(\mathbf{H}_3|\mathbf{H}_1)$ from height configuration $\mathbf{H}_1$ to configuration $\mathbf{H}_3$ in the time interval $t+t'$,

$$T_{t+t'}(\mathbf{H}_3|\mathbf{H}_1) = \sum_{\mathbf{H}_2} T_{t'}(\mathbf{H}_3|\mathbf{H}_2) T_t(\mathbf{H}_2|\mathbf{H}_1), \tag{1}$$

where $t=t_2-t_1$ and $t'=t_3-t_2$. The differential form of this equation, expressed in terms of the small-time limit of the transition probability, is the master equation [55]

$$\frac{\partial P}{\partial t} = \sum_{\mathbf{r}} [W(\mathbf{H}-\mathbf{r};\mathbf{r})P(\mathbf{H}-\mathbf{r},t) - W(\mathbf{H};\mathbf{r})P(\mathbf{H},t)], \tag{2}$$

where $P(\mathbf{H},t) \equiv T_t(\mathbf{H}|\mathbf{H}_1)$, $W(\mathbf{H};\mathbf{r})$ is the transition rate from $\mathbf{H}$ to $\mathbf{H}+\mathbf{r}$, and $\mathbf{r}=\{r_1, r_2, \ldots, r_L\}$ is the array of jump lengths between height configurations.

As a simple illustration, consider the deposition of particles onto randomly chosen lattice sites at a rate τ_0^{-1}, with the particles always remaining at the original deposition site. For this process the transition rate is given by

$$W_1(\mathbf{H};\mathbf{r}) = \tau_0^{-1} \sum_i \delta_{r_i,a_\perp} \prod_{k\neq i} \delta_{r_k,0}, \tag{3}$$

where $\delta_{i,j}$ is the Kronecker delta and $a_\perp$ is the perpendicular lattice spacing. Transition rates for deposition processes which include instantaneous local particle movements, activated transition processes, or processes leading to the removal of particles from the system can be found in Refs. [49,50,56,57].

The Chapman-Kolmogorov equation (1) is the definitive statement of the evolution of Markovian lattice models and is solved implicitly when performing computer simulations. The master equation (2) is a formal restatement of the Chapman-Kolmogorov equation in terms of a continuous time variable, but with discrete height variables. Although the master equation is more manageable than the Chapman-Kolmogorov equation, many nonequilibrium systems, such as driven surfaces [58,59], only allow a direct solution for a few special cases. We develop a more flexible computational framework based on the Kramers-Moyal-van Kampen expansion [42,49,55] and implementations of limit theorems due to Kurtz [60–68] to obtain a Fokker-Planck equation that embodies the statistical properties of the master equation. The Fokker-Planck and its associated Langevin equation are formulated in terms of continuous time and height variables that bear a definite relationship to the original discrete variables used in Eq. (1).

The Kramers–Moyal–van Kampen expansion relies [55] on the expansion of the first term on the right-hand side of Eq. (2) in terms of the jump length $\mathbf{r}$. For this purpose we identify the "largeness" parameter Ω governing intrinsic fluctuations [55] as the reciprocal of the particle size or deposition unit [48,49]. Transforming to the continuous height and time variables $h_i' = \Omega^{-1} H_i$ and $\tau' = \Omega^{-1} t$, we obtain the master equation

$$\frac{\partial P}{\partial \tau'} = \int [\tilde{W}(\mathbf{h}'-\mathbf{r};\mathbf{r})P(\mathbf{h}'-\mathbf{r},\tau') - \tilde{W}(\mathbf{h}';\mathbf{r})P(\mathbf{h}',\tau')] d\mathbf{r}, \tag{4}$$

where the $\tilde{W}$ are transition rate densities for jumps rescaled by Ω relative to the original lattice model, which satisfy smoothness and small-jump conditions [49,55].

Suitable representations of $\tilde{W}$ are obtained by extending the transition rules of lattice models to continuous variables. In some situations the $\tilde{W}$ are straightforward generalizations of the corresponding discrete transition rates [56,64–66]. For instance, the transition rate for random deposition in Eq. (3) becomes

$$\tilde{W}_1(\mathbf{h}';\mathbf{r}) = \tau_0^{-1} \Omega \sum_i \delta\left(r_i - \frac{a_\perp}{\Omega}\right) \prod_{j\neq i} \delta(r_j), \tag{5}$$

where $\delta(x)$ is the Dirac delta function. But for lattice models that have threshold character, obtaining expressions for $\tilde{W}$ is more subtle [49,50,57]. Consider, for example, the nearest-neighbor coordination number n_i, calculated by determining how many nearest neighbors of site i have heights greater than or equal to H_i,

$$n_i = \theta_d(H_{i-1} - H_i) + \theta_d(H_{i+1} - H_i), \tag{6}$$

in which the discrete step function θ_d is given by

$$\theta_d(\Delta H) = \begin{cases} 1 & \text{if } \Delta H \geqslant 0, \\ 0 & \text{if } \Delta H < 0, \end{cases} \tag{7}$$

for *discrete* height differences ΔH. For *continuous* height differences Δh we represent θ_d by

$$\theta(\Delta h;\delta) = \frac{1}{2a}\int_{-\infty}^{a_\perp^{-1}\Delta h} [\mathrm{erf}((s+a)\delta) - \mathrm{erf}(s\delta)]ds, \tag{8}$$

where $\mathrm{erf}(x)$ is the error function, $0 < a \leqslant 1$, and $\delta > 0$. The form of θ in Eq. (8) will be discussed in greater detail in Sec. II B. For now we note that we can define

$$\theta(\Delta h) = \frac{1}{a}[\max(a_\perp^{-1}\Delta h + a, 0) - \max(a_\perp^{-1}\Delta h, 0)], \tag{9}$$

where $\max(x)$ is the maximum function, such that

$$\lim_{\delta\to\infty} \theta(\Delta h;\delta) = \theta(\Delta h) \quad \text{for any } \Delta h, \tag{10}$$

$$\lim_{\delta\to\infty} \theta(\Delta H;\delta) = \theta_d(\Delta H) \quad \text{for any integer } \Delta H. \tag{11}$$

The replacement of θ_d by θ renders the transition rates continuous as well, but the appropriate form of $\theta(\Delta h)$ depends on the transition rules [49,50]. For $\delta \to \infty$, these modifications amount to an *extension* of the rules of the original (discrete) lattice model to continuous height and time variables.

The master equation (4), formulated in terms of continuous variables, can be transformed [49,50,60–68] into the more analytically tractable lattice Langevin equation

$$\frac{dh_i}{d\tau} = K_i^{(1)} + \eta_i, \tag{12}$$

for $i = 1, 2, \ldots, L$, where we have restored the original scale of the height and time variables through $h_i' \to h_i = \Omega h_i'$ and $\tau' \to \tau = \Omega\tau'$, $K_i^{(1)}$ is the first moment of the transition rate density, and the η_i are Gaussian noises that have zero mean and covariances

$$\langle \eta_i(\tau_1)\, \eta_j(\tau_2)\rangle = K_{ij}^{(2)}\delta(\tau_1 - \tau_2), \tag{13}$$

in which $K_{ij}^{(2)}$ is the second moment of the transition rate density. The transition moments are defined by

$$K_i^{(1)}(\mathbf{h}) = \int r_i W(\mathbf{h};\mathbf{r}) d\mathbf{r}, \tag{14}$$

$$K_{ij}^{(2)}(\mathbf{h}) = \int r_i r_j W(\mathbf{h};\mathbf{r}) d\mathbf{r}, \tag{15}$$

where W is the rescaled representation of $\tilde{W}$ appropriate for h_i and τ. For random deposition, for instance, we have the continuum representation

$$W_1(\mathbf{h};\mathbf{r}) = \tau_0^{-1}\sum_i \delta(r_i - a_\perp)\prod_{j\neq i}\delta(r_j). \tag{16}$$

This expression is a straightforward generalization of Eq. (3) because the updating rule does not involve particle numbers at any lattice sites apart from the deposition site.

As noted above, Eq. (12) can be obtained from a Kramers–Moyal–van Kampen expansion [55] of the master equation or from Kurtz's theorems [60–68]. The Kramers–Moyal–van Kampen expansion of lattice models [49,50,55] has been used with great success in the description of fluctuations in physical systems [55], but has several limitations [64–66] that can be overcome [64–68] by employing Kurtz's limit theorems [60–63]. The emphasis in these studies is on the transition from the discrete jumps of size Ω^{-1} in $\mathbf{h}'$ to corresponding "continuous jumps" for $\Omega \to \infty$, which allows the "control of discreteness" [64] in the system and, thus, provides a natural method for the passage from discrete to continuous variables. Accordingly, beginning with Eq. (4) and invoking Kurtz's theorems, one arrives [64–68] at Eq. (12) as $\Omega \to \infty$ under rather mild mathematical assumptions [64,68]. Contrary to the Kramers–Moyal–van Kampen expansion, no assumptions are made regarding a deterministic description or the size of the fluctuations [64,67]. Equation (12) has been used to study systems with absorbing states [64], phase transitions in the Schlögl model [65], the amplification of intrinsic noise through chaotic dynamics [67], and in various other contexts [66,69,70].

From a physical perspective, the main assumptions [64] made in the passage from Eq. (4) to Eq. (12) are that fluctuations result from the discreteness of the system, that their size is of $O(\Omega)$, and that the limit $\Omega \to \infty$ is physically reasonable. In many situations these assumptions are justified, but neither the Kramers–Moyal–van Kampen expansion nor Kurtz's theorems specify *how* to extend the transition rates to continuous variables or arbitrary $\Omega > 1$. As mentioned above, the description of stochastic lattice models defined by the Chapman-Kolmogorov equation (1) in terms of the lattice Langevin equation (12) relies crucially on finding appropriate extensions of the transition rules to continuous height and time variables. Where such extensions have been identified [49,50,57], the lattice Langevin formulation can reproduce many of the key properties of discrete stochastic lattice models [48–50,56,57,64–66]. Despite its "atomic resolution," the lattice Langevin equation (12) is simple enough to allow a direct mathematical analysis. This equation thereby provides an analytic augmentation [49] of the purely algorithmic approach taken when performing simulations of stochastic lattice models.

B. Regularized Langevin equations

This section explains how the lattice Langevin equation (12) for stochastic lattice models can be regularized to obtain a corresponding *continuum* Langevin equation. We begin by introducing the continuous space variable x and the analytic height function $u(x,\tau)$, which has the Taylor expansion

$$h(i \pm n, \tau) = \sum_{k=0}^{\infty} \left.\frac{\partial^k u}{\partial x^k}\right|_i \frac{(\pm a_\parallel n)^k}{k!}, \tag{17}$$

where $a_\parallel$ is the lateral lattice spacing. According to this expansion, all height variables that determine the first and sec-

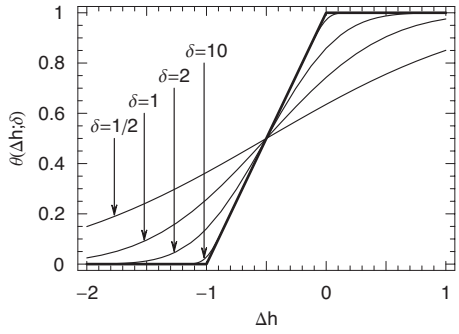

FIG. 1. Regularized step function $\theta(\Delta h;\delta)$, defined in Eq. (8), for $\delta\to\infty$ (bold line) and the indicated values of δ with $a=1$ and $a_\perp=1$.

ond moments at site i and, hence, the lattice Langevin equation (12) at this lattice site, are represented by u and its derivatives evaluated there. For many lattice models, however, height variables appear only as arguments of nonanalytic threshold functions, such as the maximum function, which can be expressed in terms of the discrete step function $\theta_d(\Delta H)$ for integer ΔH. Following Sec. II A, the description of such processes by the lattice Langevin equation necessitates representing θ_d by a continuous function θ. Comparisons [49,50,57] between computer simulations and solutions of Eq. (12) demonstrate the suitability of Eq. (8) for large δ for several lattice models. The value of a can often be determined from the transition rules in a relatively straightforward manner [49,50,57], with the result that acceptable agreement between simulations of lattice models and integrations of Eq. (12) is obtained. The regularization of θ_d in Eq. (8) is differentiable everywhere for finite δ, which makes the replacement of $h_i(\tau)$ by $u(x,\tau)$ meaningful. The function $\theta(\Delta h;\delta)$ is plotted in Fig. 1 for several values of δ.

The form of θ for $\delta\to\infty$ and, thus, the transition rates in the lattice Langevin equation (12) can be obtained from the rules of the original lattice model [49,50,57]. However, no differentiable θ, which corresponds to a finite δ in Eq. (8), can be exact, since the threshold properties of the discrete step function θ_d are necessarily violated. However, Fig. 1 suggests that θ closely approximates its limiting form for large values of δ. Indeed, by comparing the results of KMC simulations with the corresponding solutions of the lattice Langevin equation, one finds that agreement (within numerical accuracy) is obtained not only for $\delta\to\infty$ but also for a range $\delta_0<\delta<\infty$, with $\delta_0\sim 10$ a typical value. From a practical perspective we can therefore replace θ_d by θ with $\delta>\delta_0$ with minimal detrimental effect on the accuracy of the lattice Langevin equation.

The integral in Eq. (8) evaluates to

$$\theta(a_\perp\Delta h;\delta)=\frac{1}{2a}\left\{a+\frac{1}{\sqrt{\pi}\delta}[e^{-\delta^2(\Delta h+a)^2}-e^{-\delta^2(\Delta h)^2}]+(\Delta h+a)\mathrm{erf}(\delta(\Delta h+a))-\Delta h\,\mathrm{erf}(\delta\Delta h)\right\}, \tag{18}$$

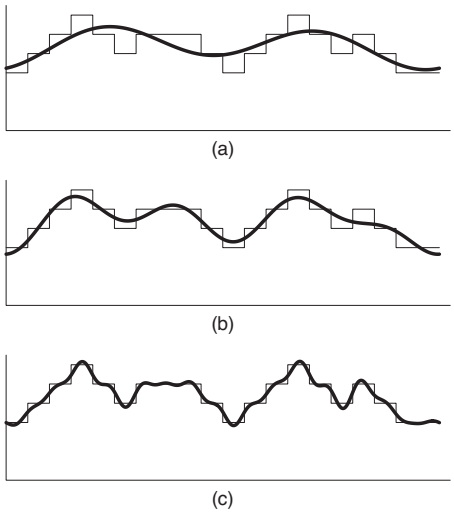

FIG. 2. Coarse graining of height configurations induced by decreasing values of δ in $\theta(\Delta h;\delta)$, with (a) $\delta\ll\delta_0$, (b) $\delta\lesssim\delta_0$, and (c) $\delta>\delta_0$. The coarse-grained profile (thick line) is shown superimposed on the heights of the underlying lattice model.

from which it is clear that the Taylor expansion of θ around $\Delta h=0$ has an infinite radius of convergence for any finite δ. This is our principal motivation for choosing this regularization. Thus, assuming δ to be finite, θ is expanded around $\Delta h=0$ as

$$\theta(\Delta h;\delta)=A(\delta;a)+\frac{B(\delta;a)}{a_\perp}\Delta h+\frac{C(\delta;a)}{a_\perp^2}(\Delta h)^2+\cdots. \tag{19}$$

The substitution of this expansion with Eq. (17) into the lattice Langevin equation (12) with $\delta_0<\delta<\infty$ yields an effective finite-order continuum equation that embodies the lattice transition rules. The convergence of the Taylor expansion of θ thereby guarantees that corrections to this continuum equation are small and can be included systematically.

An altogether different scenario arises if $\delta<\delta_0$ in $\theta(\Delta h;\delta)$. As can be seen from Fig. 1, for small δ the regularization θ smears out relative height differences and the Langevin equation no longer captures the atomic-scale details of the lattice model (Fig. 2). As a result, however, the gradient of θ is reduced, which means that the expansion of θ in Eq. (19) converges rapidly and the rules of the lattice model, which enter through the form and symmetry of the transition moments, already manifest themselves within the first few orders of the continuum equation. Choosing $\delta<\delta_0$ therefore changes the *quantitative* but not the *qualitative* features of the surface morphology and, in particular, retains basic morphological properties such as the dynamic scaling behavior. This will be illustrated in Sec. IV.

The continuum limit of the lattice Langevin equation (12) can therefore be taken in two ways. On the one hand, for $\delta_0<\delta<\infty$ one obtains an essentially exact large-order continuum equation [Fig. 2(c)]. This equation can be solved numerically to a prescribed tolerance by checking the local gra-

dients after each iteration and, if necessary, including higher-order terms in the computation. The expansion of θ for $\delta < \delta_0$, on the other hand, yields terms which determine fundamental properties of the lattice model, such as the scaling behavior [Fig. 2(b)]. For our purposes, higher-order terms describing small-wavelength behavior represent redundant information because under RG transformations irrelevant higher-order terms "collapse" onto leading-order terms, and information about such higher-order corrections is thus effectively lost under coarse graining. We will therefore focus on the case $\delta < \delta_0$.

For some value of δ the lowest-order continuum equation that can produce the scaling behavior of the lattice model is obtained. This places the upper bound δ' on the value of δ which, in general, depends on the lattice model and the substrate dimension. If the dominant terms in the continuum equation for $\delta \sim \delta'$ are linear, decreasing δ further does not change the dominance of these terms. On the other hand, if the coefficients of nonlinear terms take appreciable magnitudes for $\delta \sim \delta'$, letting $\delta \to 0$ artificially suppresses these terms [Fig. 2(a)]. This is seen most directly from Eq. (19) by noting that as $\delta \to 0$ we have $A \to 0.5$ and all other coefficients approach 0, with $C/B \to 0$. More generally, the coefficient of $(\Delta h)^n$ in Eq. (19) is proportional to δ^n if $n=1,3,\ldots$ and proportional to δ^{n+1} if $n=2,4,\ldots$ as $\delta \to 0$. In some circumstances nonlinear terms are therefore suppressed relative to linear terms as $\delta \to 0$, and it can be quite subtle to obtain suitable values for δ which produce the leading-order equation for a given lattice model. This important point is discussed further in Sec. III and, for specific lattice models, in Sec. IV and Refs. [47,50].

The substitution of Eqs. (17) and (19) with $\delta < \delta'$ into the lattice Langevin equation (12) produces the leading-order continuum equation describing the fundamental properties of a given lattice model. For lattice models of homoepitaxial growth, the processes typically included are some combination of random deposition or random deposition followed by rapid nonthermal relaxation and nearest-neighbor thermally activated hopping. For such models, we find [45–47,50] that the leading-order continuum Langevin equation is

$$\frac{\partial u}{\partial \tau} = \nu_2 \nabla^2 u - \nu_4 \nabla^4 u + \lambda_{13} \nabla (\nabla u)^3 + \lambda_{22} \nabla^2 (\nabla u)^2 + \xi, \tag{20}$$

where the Gaussian noise $\xi(x,\tau)$ has zero mean and covariance

$$\langle \xi(x_1,\tau_1)\xi(x_2,\tau_2)\rangle = 2\mathcal{D}\delta(x_1-x_1)\delta(\tau_1-\tau_2), \tag{21}$$

in which $\mathcal{D}=D_0-D_2\nabla^2$. In writing the continuum Langevin equation (20) we have made the transformation $u \to u + a_\perp \tau$ to eliminate the absolute average height of the surface profile, so that u describes the *fluctuations* about this average.

Other types of terms can also be present. For example, environment-dependent evaporation processes or amorphous growth lead to the presence of terms that cannot be represented as the divergence of a surface current [42,50,57,71] and some types of local-environment-dependent hopping found in models of heteroepitaxy [72] lead to the presence of other linear and nonlinear terms that preempt scale invariance. But our interest here is in conserved models for which Eqs. (20) and (21) provide a generic continuum description. The numerical values of the coefficients in these equations are determined by the rules of the underlying lattice model and the substrate dimension. In Sec. IV we compile the values of the coefficients obtained for the 1D WV model. The corresponding values for other lattice models described by Eqs. (20) and (21) can be found in Refs. [45–47,50]. The coefficients of higher-order corrections to Eq. (20) have magnitudes that make them negligible in comparison to the terms that have been retained [47,50].

The basic assumption in the passage from Eq. (12) to Eq. (20) is that the lattice Langevin equation can be regularized and expanded as a convergent Taylor series in the sense that the coefficients of higher-order derivatives diminish rapidly in magnitude. The order of the terms retained in Eq. (20) is determined by the magnitudes and signs of the coefficients. There are lattice models for which the lowest-order terms in the expansion of Eq. (12) are dominant even at atomistic scales [47,50,71]. But there are also models for which terms beyond fourth order in the spatial derivatives must be retained, either because the coefficients of such higher-order terms are of comparable magnitude to those of lower order or for reasons of stability [72]. Moreover, there are also scenarios [73] where the form of the continuum description suggests that an altogether different approach for taking the continuum limit of Eq. (12), such as a (partial) resummation of the expansion of the lattice Langevin equation, might be required.

The general form of the Langevin equation (20) has been previously postulated on the basis of symmetry arguments [1,24] and subsumes several widely studied continuum equations of conserved surface growth as special cases: the Edwards-Wilkinson (EW) equation [28]

$$\frac{\partial u}{\partial \tau} = \nu_2 \nabla^2 u + \xi, \tag{22}$$

the Mullins-Herring (MH) equation [26,27]

$$\frac{\partial u}{\partial \tau} = -\nu_4 \nabla^4 u + \xi, \tag{23}$$

the Villain-Lai-Das Sarma (VLDS) equation [24,30]

$$\frac{\partial u}{\partial \tau} = -\nu_4 \nabla^4 u + \lambda_{22} \nabla^2 (\nabla u)^2 + \xi, \tag{24}$$

and the equation

$$\frac{\partial u}{\partial \tau} = -\nu_4 \nabla^4 u + \lambda_{13} \nabla (\nabla u)^3 + \xi, \tag{25}$$

studied in Ref. [74]. The justification of these equations for particular growth scenarios typically relies on phenomenological and scaling arguments [1,24] to eliminate some of the terms in Eq. (20). Our analysis [45] suggests, however, that *all* terms in Eq. (20) generally have nonzero coefficients for homoepitaxial growth, at least at finite length and time scales. Hence, the complete equation (20) must be used when making comparisons between continuum descriptions and

computer simulations of lattice models or experiments, which access only transient regimes. Differences in the transition rules of lattice models of homoepitaxial growth enter through the relative magnitudes and signs of the coefficients [45–47,50] in the leading-order equation (20). Indeed, as discussed in Sec. IV, the inclusion of all these terms, as well as the relative magnitudes and signs of the coefficients, is of paramount importance for obtaining the correct renormalization behavior of the WV model.

III. COARSE-GRAINED LANGEVIN EQUATIONS

Taking the continuum limit of the lattice Langevin equation (12) according to the procedure described in Sec. II B yields an atomic-scale stochastic partial differential equation for the lattice model under consideration. For $\delta > \delta_0$ this equation represents a faithful embodiment of the lattice rules, while for $\delta < \delta'$ only the fundamental properties of the lattice model are retained. The properties of this equation can be ascertained by direct numerical integration or with analytic methods used in statistical dynamics [1,22–25,75,76]. The crucial point is that the continuum Langevin equation retains, via the lattice Langevin equation and its antecedent, the Chapman-Kolmogorov equation, a direct connection to the transition rules of the original lattice model.

In Sec. III A we briefly review some of the general aspects of the RG and provide an illustration in the context of homoepitaxial growth. Section III B describes how the derivation of continuum Langevin equations from the transition rules of lattice models (Sec. II) can be combined with the RG to obtain a multiscale theory of stochastic lattice models.

A. Renormalization-group equations

We will use the *dynamic* RG to investigate the multiscale behavior of lattice models. The dynamic RG procedure is an extension of the standard RG to time-dependent systems, which are typically formulated as differential equations, and consists of two basic steps [23,77–81]. In the first step, degrees of freedom associated with small length scales are integrated out and averaged over. Absorbing the contributions of these degrees of freedom into a redefinition of the parameters in the differential equation leads to "intermediate" RG equations for the coefficients in the differential equation. In the second step, the spatial variable is rescaled to its original range, with a corresponding rescaling of all other physical quantities in the model. Carrying out this procedure over infinitesimal momentum shells leads to the differential RG flow equations of the system.

The RG is perhaps most widely applied to the study of systems in the macroscopic limit of arbitrarily large length and time scales. If such a macroscopic description exists, it must clearly be invariant under the RG. Possible macroscopic descriptions of the system are therefore the fixed points of the RG equations. In the case of the dynamic RG a continuum Langevin equation is associated with each fixed point. At a fixed point of the RG the coefficients in the Langevin equation are constant and, hence, the values of the scaling exponents must also take constant numerical values to compensate for the "thinning" of degrees of freedom in the first step of the RG. As a result, a set of scaling exponents characterizing the geometry of the system is associated with each fixed point.

The domain of attraction of a given fixed point—the "critical" surface in the language of critical phenomena—defines a set of initial conditions which yield this fixed point at macroscopic scales. In the macroscopic limit a large number of microscopic descriptions therefore leads to an identical macroscopic description characterized by a set of scaling exponents. This is referred to as universality. But while the experimental observation of universality proved to be a crucial test for the RG, the framework for coarse graining provided by the RG is not limited to the analysis of fixed points [81] because RG equations are valid for *any* scale. Thus, the RG allows [81,82] the study of systems at finite distances from fixed points and, as a result, the analysis of the competition between different fixed points [81,83,84], a phenomenon known as crossover. For some cases, the general nonlinear solutions of the RG equations have been obtained [81–85], in which case it is possible to study crossover for general initial conditions of RG transformations.

The RG calculation described in this paper was performed using two complementary formulations: the standard diagrammatic approach [23,77,80] and irreducible differential generators [81]. The diagrammatic method is based on rules for combining the terms in a continuum Langevin equation into a diagram that describes the perturbative effects of interactions. This allows a direct comparison with previous RG calculations for growth equations [22–25,29,74,86]. The generator method, on the other hand, is founded on the expansion of a closed-form functional equation that yields the same expressions as the diagrammatic method, including symmetry factors, and thus serves as an independent check of the diagrammatic calculations. We describe below the application of the RG to homoepitaxial surface growth.

1. Renormalization group for homoepitaxial growth

In Sec. II B it was found that prototype lattice models for homoepitaxial growth are described by the leading-order continuum Langevin equation (20) with the noise covariance in Eq. (21). In this section we summarize the RG analysis of this equation. The outcome of this procedure is a system of ordinary differential equations describing how the coefficients in Eqs. (20) and (21) change under repeated coarse graining (Appendix A and Ref. [50]). We find that the noise covariance is modified to $\mathcal{D}=D_0-D_2\nabla^2+D_4\nabla^4$ [25] and that the coefficients in Eq. (20) renormalize under the change of scale $\mathbf{x}\to e^{d\ell}\mathbf{x}$, $\tau\to e^{zd\ell}\tau$, and $u\to e^{\alpha d\ell}u$ to one-loop order according to

$$\frac{d\nu_2}{d\ell} = (z-2)\nu_2 + K_d\frac{d+2}{d}\frac{\lambda_{13}D\Lambda^d}{\nu}, \tag{26}$$

$$\frac{d\nu_4}{d\ell} = (z-4)\nu_4 - \frac{K_d}{d}\frac{\lambda_{22}^2 D_s\Lambda^d}{\nu^3}, \tag{27}$$

$$\frac{d\lambda_{13}}{d\ell} = (z-4+2\alpha)\lambda_{13} - \frac{AK_d}{d(d+2)}\frac{\lambda_{13}^2 D\Lambda^d}{\nu^2}, \tag{28}$$

$$\frac{d\lambda_{22}}{d\ell} = (z-4+\alpha)\lambda_{22} - 2K_d\frac{d+2}{d}\frac{\lambda_{13}\lambda_{22}D\Lambda^d}{\nu^2}, \tag{29}$$

$$\frac{dD_0}{d\ell} = (z-d-2\alpha)D_0, \tag{30}$$

$$\frac{dD_2}{d\ell} = (z-d-2\alpha-2)D_2, \tag{31}$$

$$\frac{dD_4}{d\ell} = (z-d-2\alpha-4)D_4 + K_d\frac{\lambda_{22}^2 D^2\Lambda^{d-2}}{\nu^3}, \tag{32}$$

where $K_d=S_d/(2\pi)^d$, $S_d=2\pi^{d/2}/\Gamma(\frac{1}{2}d)$ is the surface area of a d-dimensional unit sphere, Λ is the momentum cutoff, and

$$A = d^2+6d+20, \tag{33}$$

$$\nu = \nu_2 + \nu_4\Lambda^2, \tag{34}$$

$$D = D_0 + D_2\Lambda^2 + D_4\Lambda^4, \tag{35}$$

$$D_s = \sum_{i=0}^{2}[(d-4+2i)\nu - 2\nu_4\Lambda^2]D_{2i}\Lambda^{2i}. \tag{36}$$

The flow parameter ℓ in Eqs. (26)–(32) determines the degree of coarse graining between microscopic ($\ell=0$) and macroscopic ($\ell\to\infty$) regimes. The general form of the one-loop contributions in the RG equations (26)–(32) can be verified by dimensional analysis [50].

The RG equations (26)–(32) agree in almost every respect with those obtained in previous calculations of related problems [24,25,29,74,86,87]. However, there is an inconsistency between the equations for ν_4 in Refs. [24] and [25,29]: Equation (8a) in Ref. [24] differs by a factor of 4 from Eq. (3) in Ref. [29] and Eq. (12a) in Ref. [25], despite the fact that the flow equations in Refs. [24,25] and Ref. [29] should be identical up to the difference in the factors of $(6-d)$ versus $(4-d)$, due to different definitions of the noise [88]. The Feynman graph in question is calculated in Appendix A, where we obtain agreement with the corresponding flow equation in Refs. [25,29]. There is also an inconsistency between the flow equations for ν_2 and λ_{13} in Refs. [86,87], which should differ only in the dimensions of the coefficients. Our calculation [50] supports the result in Ref. [86]. If the results reported in Refs. [25,29,86] are correct, the flow equations (26)–(32) agree with the previous calculations noted above.

Equation (30) shows that the noise covariance D_0 does not renormalize to one-loop order—the changes to this quantity are due only to scale changes. This implies that the scaling relation

$$z - 2\alpha = d \tag{37}$$

must be satisfied. Since the deterministic part of the Langevin equation (20) is conserved, whereas D_0 is the covariance of nonconserved shot noise, this scaling relation is, in fact, exact to any order in perturbation theory [25]. This conclusion also follows by noting that the value of D_0 in the atomic-scale equation (20) is proportional to the deposition flux [45,46]. Since the deterministic part of this equation conserves the particle number, the growth rate and, hence, the value of D_0 must be the same at any scale, which implies Eq. (37). Nonconserved lattice models, on the other hand, renormalize according to the RG equations of the Kardar-Parisi-Zhang universality class [22,23], in which case Eq. (37) does not hold.

2. Transformation of renormalization-group equations

The solution of Eqs. (26)–(32) yields RG trajectories in the space of the six coefficients ν_2, ν_4, λ_{13}, λ_{22}, D_2, and D_4, with D_0 remaining constant on account of Eq. (37). The calculation and visualization of these trajectories is simplified considerably by transforming to the dimensionless quantities

$$r = \frac{\nu_4\Lambda^2}{\nu_2+\nu_4\Lambda^2}, \tag{38}$$

$$u_1 = K_d\frac{3d^2+14d+28}{d^2(d+2)}\frac{D_0\lambda_{13}\Lambda^d}{(\nu_2+\nu_4\Lambda^2)^2}, \tag{39}$$

$$u_2 = \left[K_d\frac{3(6-d)}{d(4-d)}\frac{D_0\lambda_{22}^2\Lambda^{d+2}}{(\nu_2+\nu_4\Lambda^2)^3}\right]^{1/2}, \tag{40}$$

$$\Gamma_2 = \frac{D_2\Lambda^2}{D_0}, \tag{41}$$

$$\Gamma_4 = \frac{D_4\Lambda^4}{D_0}, \tag{42}$$

in terms of which the RG equations (26)–(32) reduce to [50]

$$\frac{dr}{d\ell} = -2r(1-r) - 2Bru_1\Gamma + 2C(1-r)u_2^2\Gamma_s, \tag{43}$$

$$\frac{du_1}{d\ell} = u_1(-d+4r-du_1\Gamma - 4Cu_2^2\Gamma_s), \tag{44}$$

$$\frac{du_2}{d\ell} = u_2\left[-\frac{1}{2}(d+2)+3r-7Bu_1\Gamma - 3Cu_2^2\Gamma_s\right], \tag{45}$$

$$\frac{d\Gamma_2}{d\ell} = -2\Gamma_2, \tag{46}$$

$$\frac{d\Gamma_4}{d\ell} = -4\Gamma_4 + 2dCu_2^2\Gamma^2, \tag{47}$$

where $\Gamma=1+\Gamma_2+\Gamma_4$,

TABLE I. Fixed points of the transformed RG equations (43)–(47). In these expressions i is the complex unit such that $i^2=-1$.

Fixed point	d	r	u_1	u_2	Γ_2	Γ_4
Edwards-Wilkinson (EW)	any	0	0	0	0	0
Mullins-Herring (MH)	any	1	0	0	0	0
Fixed point 1 (FP1)	any	0	-1	0	0	0
Fixed point 2 (FP2)	$d=1$	$\frac{3}{2}$	5	0	0	0
	$d=2$	$\frac{13}{9}$	$\frac{17}{9}$	0	0	0
	$d=3$	$\frac{119}{94}$	$\frac{97}{141}$	0	0	0
Villain-Lai-Das Sarma$^+$ (VLDS$^+$)	$d=1$	1	0	± 0.99	0	0.055
	$d=2$	1	0	± 1	0	0.10
	$d=3$	1	0	± 1.0	0	0.11
Villain-Lai-Das Sarma$^-$ (VLDS$^-$)	$d=1$	1	0	$\pm 2.2i$	0	-6.1
	$d=2$	1	0	± 1	0	9.9
	$d=3$	1	0	± 1.6	0	1.9
Fixed point 3^+ (FP3^+)	$d=1$	$\frac{8}{5}$	-11	$\pm 5.0i$	0	-2.4
	$d=2$	3	$-0.76i$	$\pm 1.3 \pm 1.0i$	0	$-1-4.5i$
	$d=3$	$\frac{8}{13}$	$-0.39+0.088i$	$\pm 1.7 \pm 0.26i$	0	$0.32+0.29i$
Fixed point 3^- (FP3^-)	$d=1$	$\frac{8}{5}$	18	$\pm 2.0i$	0	-0.15
	$d=2$	3	$0.76i$	$\pm 1.3 \mp 1.0i$	0	$-1+4.5i$
	$d=3$	$\frac{8}{13}$	$-0.39-0.088i$	$\pm 1.7 \mp 0.26i$	0	$0.32-0.29i$

$$\Gamma_s = 4 - d + 2r + \Gamma_2(2 - d + 2r) + \Gamma_4(-d + 2r), \quad (48)$$

and

$$B = \frac{d(d+2)^2}{2(3d^2+14d+28)}, \quad C = \frac{4-d}{6(6-d)}. \quad (49)$$

The transformed RG flow equations (43)–(47) are especially well suited to the multiscale analysis of the Langevin equation (20), for three main reasons. First, Eqs. (43)–(47) are independent of the scaling exponents α and z. This simplifies the investigation of crossover regimes, for which the scaling exponents are not known *a priori*. Second, in terms of the dimensionless quantities in Eqs. (38)–(42) the subspace of the parameter space spanned by ν_2, ν_4, λ_{13}, λ_{22}, D_0, D_2, and D_4, which determines the behavior of the deterministic part of Eq. (20), has three dimensions (r,u_1,u_2). The interplay between the linear and nonlinear terms governing the deterministic behavior of the lattice model can therefore be visualized in a three-dimensional diagram. Finally, the transformed RG equations are simple enough to allow the solution for all fixed points of lattice models described by Eq. (20). This is discussed in the next section.

3. Fixed points of homoepitaxial growth

The fixed points of Eqs. (43)–(47) are obtained in the standard manner [89] by solving $dr/d\ell=0$, $du_i/d\ell=0$, and $d\Gamma_j/d\ell=0$ for $i=1,2$ and $j=2,4$. The details of this lengthy calculation are described in Ref. [50] and the outcome summarized in Table I. There are 12 fixed points, which we divide into six different categories according to the form of the continuum Langevin equation associated with the fixed point. Expressions for fixed point 2 (FP2), the Villain-Lai-Das Sarma$^\pm$ (VLDS$^\pm$) fixed point, and fixed point $3^\pm$ (FP$3^\pm$) for any dimensions can be found in Appendix B.

The EW fixed point corresponds to the EW equation (22), the MH fixed point to the MH equation (23), and the VLDS$^\pm$ fixed point to the VLDS equation (24). The Gaussian noise in these equations has zero mean and the covariance in Eq. (21) with $D_2=0$. For the EW and MH fixed points we also have $D_4=0$, whereas $D_4\neq 0$ at the VLDS fixed point [25]. Distinct scaling exponents are associated with each fixed point [1]. Although D_4 is nonzero for some fixed points in Table I, such as the VLDS fixed point, a finite D_4 only shifts the location of fixed points through a modification of D and D_s in Eqs. (26)–(32), but does not affect the scaling behavior [25]. We note, however, that Eq. (25) studied in Ref. [74] is not associated with any fixed point. This is because the term $\lambda_{13}\nabla(\nabla u)^3$ automatically generates the term $\nu_2\nabla^2 u$ under RG transformations [74], which dominates over $-\nu_4\nabla^4 u$ in the scaling sense.

Widely studied variations of Eqs. (23) and (24) are the *conserved* MH (cMH) equation [1] and the *conserved* VLDS (cVLDS) equation [29], for which $D_0=0$ and $D_2\neq 0$. This corresponds to $\Gamma_2\to\infty$ in our formalism. In view of Eqs. (26)–(32) and the scaling relation in Eq. (37), no fixed point with conserved noise can be obtained if $D_0(\ell=0)\neq 0$, which has the physical interpretation of a nonzero deposition flux in lattice models for surface growth. However, even for a finite deposition flux the cMH equation and the cVLDS equation can govern the *transient* behavior of lattice models [45–47,50].

Fixed point 1 is also mentioned in Ref. [87] and corresponds to an equation of the form

$$\frac{\partial u}{\partial \tau} = \nu_2 \nabla^2 u - \lambda_{13} \nabla (\nabla u)^3 + \xi, \tag{50}$$

which, considering the form of the flow equations (26)–(32), is stable under RG transformations due to the competing effects of ν_2 and λ_{13}. The Langevin equation associated with FP2 takes the form

$$\frac{\partial u}{\partial \tau} = \nu_2 \nabla^2 u - \nu_4 \nabla^4 u + \lambda_{13} \nabla (\nabla u)^3 + \xi, \tag{51}$$

where either $\nu_2 < 0$ and $\nu_4 > 0$ or $\nu_2 > 0$ and $\nu_4 < 0$. This implies that some modes of u are unstable and, if $\nu_4 < 0$, Eq. (51) is not mathematically well posed. Finally, FP3 corresponds to an equation of the form

$$\frac{\partial u}{\partial \tau} = \nu_2 \nabla^2 u - \nu_4 \nabla^4 u + \lambda_{13} \nabla (\nabla u)^3 + \lambda_{22} \nabla^2 (\nabla u)^2 + \xi, \tag{52}$$

which, for $\nu_4 < 0$, is not mathematically well posed. Moreover, some of the coefficients in Eq. (52) can take complex values, and, hence, we do not attribute any physical significance to FP3 in the context of homoepitaxy.

As noted earlier, a given fixed-point Langevin equation provides a universal description for phenomena governed by microscopic Langevin equations that fall within the domain of attraction of this fixed point. For the fixed points in Table I we find that only the EW fixed point is globally stable for the physically relevant cases $d=1,2,3$, as determined by the fixed-point eigenvalues [89]. Thus, the other fixed points can be stable only in subspaces spanned by ν_2, ν_4, λ_{22}, λ_{13}, D_0, D_2, and D_4 and are expected to govern the asymptotic behavior of the Langevin equation (20) only if some terms vanish at microscopic scales, possibly on symmetry grounds. In this context we note that there are two fixed points corresponding to the VLDS equation, VLDS$^+$ and VLDS$^-$, which, for $d=2$, differ by the value of D_4 at the fixed point. In the subspace $\nu_2=0$ and $\lambda_{13}=0$, the VLDS$^+$ fixed point is stable, whereas VLDS$^-$ is unstable. Hence, asymptotic behavior consistent with the VLDS equation, which has been observed in various computer simulations [1,24,29,54,75], corresponds to VLDS$^+$. This conclusion is consistent with the fact that for $d=1$ the coefficients at the VLDS$^-$ fixed point take unphysical values.

B. Solution of renormalization-group equations

As illustrated in Sec. III A 3, the leading-order continuum Langevin equation describing a lattice model can admit many fixed points. Although in the case of the Langevin equation (20) only one fixed point is found to be stable asymptotically, the other fixed points can still determine (arbitrarily long) transient regimes. In particular, if the RG trajectory lingers near a fixed point, the qualitative features of the lattice model can be approximately described by the scaling exponents, or some other characteristic property, of the Langevin equation associated with that fixed point, until the trajectory takes the system to another region of parameter space. Moreover, there is also the possibility that no fixed point is approached asymptotically. Thus, for theoretical as well as practical reasons it can be crucial to determine the RG trajectories of atomistic models by solving the RG equations, which is the approach we follow below.

Our multiscale theory consists of three key elements: (i) lattice models are formulated in terms of lattice Langevin equations, (ii) the Langevin equations are expressed as atomic-scale continuum equations, which is achieved through the truncation of the Taylor expansions of the fluctuating fields, and (iii) RG transformations of the atomic-scale equations yield coarse-grained continuum equations describing lattice models at arbitrary space and time scales. Thus, we first derive a microscopic continuum representation of the atomistic dynamics and then employ the RG to systematically "weed out" terms which become irrelevant at successively larger scales and absorb their effect into modified values of the remaining coefficients. In the remainder of this section we will consider the implementation of this approach for lattice transition rules involving nonanalytic threshold functions. Section 4 provides an illustration of our method for the 1D WV model.

1. Large-order multiscale theory

As discussed in Sec. II, the step function θ_d appearing in the transition rules of numerous lattice models can be regularized by the representation in Eq. (8). The range of the parameter δ is thereby partitioned into two intervals. For $\delta > \delta_0$ the regularization is essentially exact [Fig. 2(c)], as demonstrated by comparing solutions of lattice Langevin equations with computer simulations. Since the Taylor expansion of the regularized step function converges, the continuum limit of the lattice Langevin equation (see Sec. II B) yields a stochastic differential equation with a large but finite number of terms even for $\delta > \delta_0$. Solutions of this equation approximate those of the original lattice equation to any desired accuracy—for greater accuracy higher-order terms can always be included. In principle, the coefficients in the large-order equation could be used as initial conditions for nonperturbative RG transformations. This would provide the basis for a *large-order multiscale theory* that encompasses the description of lattice models from the details of atomic-scale transitions to their asymptotic scaling.

2. Leading-order multiscale theory

The rules of lattice models are often too complex to allow the implementation of the large-order multiscale theory outlined above, and a technically less demanding alternative becomes essential. To this end we note that for small enough values of $\delta < \delta_0$, one obtains a leading-order continuum equation that captures only the fundamental properties of the lattice model [Fig. 2(b)], such as the scaling behavior (see Sec IV). As shown in Sec. IV and Refs. [46,47,50], such leading-order equations do not necessarily involve only the lowest-order derivatives describing the system under consideration. The coefficients in the leading-order equation then serve as initial conditions for perturbative RG transformations, yielding a description of the lattice model at all length and time scales. This forms the basis for a *leading-order multiscale theory* of lattice models.

Such a theory has two main limitations. On the one hand, it is very difficult, if not impossible, to quantify how closely the leading-order equation describes the lattice model. In general, the leading-order equation will not accurately capture the numerical values of the fluctuating field, but only its basic properties. On the other hand, perturbative RG transformations always carry the caveat that higher-order terms in the number of loops are neglected. Such terms almost certainly shift the location of fixed points and the paths of RG flows. But despite these problems, there are fundamental reasons why one can expect accurate predictions from the leading-order theory: it captures the symmetries of the couplings in the lattice model, determines which terms dominate at atomistic scales, and provides estimates for the coefficients. Moreover, the essential property of RG transformations is that they take account of the coupling of length and time scales through nonlinear terms. This is already achieved at one-loop order.

Thus, the leading-order method introduces inherent uncertainties through the choice of $\delta < \delta_0$ and the subsequent perturbative RG transformations. The leading-order equation is obtained by demanding that the order of the dominant terms does not decrease as δ is decreased. This determines the upper bound δ', but only specifies a range of possible δ. In many instances all choices below this upper bound yield essentially identical RG trajectories [45–47,50]. For some models, however, different behavior under RG transformations can be obtained depending on the choice for $\delta < \delta'$ (see Sec. IV). In this case there are two ways to proceed: Either higher-order terms are included in the atomistic Langevin equation and the RG analysis or the appropriate range of δ is determined on the basis of some other considerations and/or comparisons with computer simulations.

Once the suitability of the leading-order equation and the perturbative RG are established for a lattice model, the following key applications of the leading-order theory can be envisaged: The description of transient regimes of lattice models through continuum equations [45–47,50], the formulation of direct quantitative links between *regions* (rather than points) in the parameter space and given transient or asymptotic regimes [46,50], the systematic investigation of lattice models for general model parameters [50], and the prediction of asymptotic equations of motion for given atomistic processes [45–47,50]. None of these goals can be achieved through computer simulations or postulated continuum descriptions alone. The leading-order approach outlined above provides a bridge between these two methodologies, linking discrete and continuous descriptions of atomistic models.

IV. WOLF-VILLAIN MODEL

This section provides an illustration of the multiscale method described in Secs. II and III for the WV model [51]. This model was in fact first proposed [52] as a relaxation mechanism for the epitaxial growth of group-IV semiconductors at temperatures too low to induce any thermal activity on the surface [92]. Other examples of this effect are transient mobility [93–95], ballistic impact [96,97], and downward funneling [98].

In the formulation of the model we study here [51,52], the transition rules stipulate that a particle arriving at a randomly chosen site remains there only if its coordination cannot be increased by moving to a nearest-neighbor site. Otherwise, the final deposition site is chosen randomly from nearest-neighbor sites that offer the maximum coordination. After the deposition and any instantaneous relaxation the particle is immobile. For simplicity we focus below on the WV model applied to 1D substrates. An analogous analysis of the two-dimensional WV model is described in Refs. [45,47,50].

A. Analytic formulation and continuum equation

The formulation of the lattice Langevin equation associated with the WV model amounts to the calculation of the first and second moments of the transition rate density in Eqs. (14) and (15) and the extension of the transition rules of the WV model to continuous variables through Eq. (8). The transition rate for this model can be written as [49]

$$W_2(\mathbf{H};\mathbf{r}) = \tau_0^{-1}\sum_i \left[w_i^{(1)} \delta_{r_i,a_\perp} \prod_{j\neq i} \delta_{r_j,0} + w_i^{(2)} \delta_{r_{i-1},a_\perp} \prod_{j\neq i-1} \delta_{r_j,0} + w_i^{(3)} \delta_{r_{i+1},a_\perp} \prod_{j\neq i+1} \delta_{r_j,0} \right], \tag{53}$$

where $w_i^{(k)}$ is the probability that a particle deposited at site i remains there ($k=1$), hops to site $i-1$ ($k=2$) or to site $i+1$ ($k=3$). The sum rule

$$w_i^{(1)} + w_i^{(2)} + w_i^{(3)} = 1 \tag{54}$$

ensures that the average deposition rate per site is τ_0^{-1}.

From Eq. (53) it is clear that all of the moments of W are diagonal and proportional to the first moment. In particular, Eqs. (14) and (15) evaluate to [42,49]

$$K_i^{(1)} = \frac{a_\perp}{\tau_0}[w_i^{(1)} + w_{i+1}^{(2)} + w_{i-1}^{(3)}], \tag{55}$$

$$K_{ij}^{(2)} = \delta_{ij} a_\perp K_i^{(1)}. \tag{56}$$

The formulation of the lattice Langevin equation for the WV model therefore reduces to the determination of expressions for the local deposition probabilities. The $w_i^{(k)}$ must distinguish between the $2^2 \times 3^2 = 36$ height configurations that are resolved by the 1D WV model, which are listed in Refs. [49,99]. As an example, consider the height configuration in Fig. 3(a), which has the mathematical expression

$$\theta_d(H_{i-1} - H_{i-2})\delta(H_i, H_{i-1})\delta(H_i, H_{i+1})[1 - \theta_d(H_{i+1} - H_{i+2})], \tag{57}$$

where we define $\delta(x,y)$ as

$$\delta(x,y) = \theta_d(x-y) + \theta_d(y-x) - 1. \tag{58}$$

According to the transition rules of the WV model a particle deposited at site i relaxes to site $i+1$ in the configuration in Fig. 3(a). Hence, expression (57) is assigned to the sum of configurations defining $w_i^{(3)}$.

The configuration in Fig. 3(b) provides an illustration of a noninteger height configuration resolved by the lattice

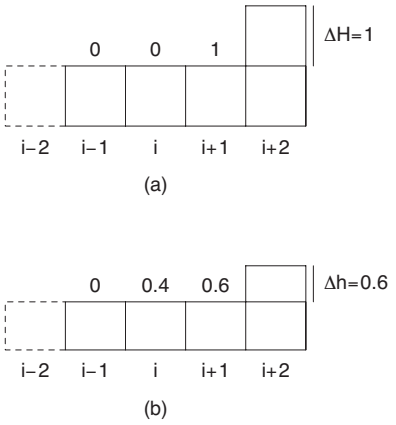

FIG. 3. Height configurations resolved by the 1D WV model for (a) integer height differences ΔH and (b) continuous height differences Δh. The numbers on top of columns $i-1$, i, and $i+1$ indicate the values of $w_i^{(2)}$, $w_i^{(1)}$, and $w_i^{(3)}$, respectively, using Eq. (9) with $a=1$ for configuration (b). Column heights strictly greater or strictly equal to adjacent sites are as shown; those less than or equal to adjacent sites are indicated with dashed lines.

Langevin equation for the WV model. The regularization in Eq. (9) with $a=1$ produces a gradual increase [49,50] in the deposition probability onto site $i+1$ as the height difference $h_{i+1}-h_i=\Delta h_{i+1}$ is increased in the interpolation range, with a corresponding decrease in the deposition probability onto site i. A "particle" encountering the configuration in Fig. 3(b) can be interpreted as relaxing according to a height difference of $\Delta h_{i+1}=1$ with probability 0.6 and according to a height difference of $\Delta h_{i+1}=0$ with probability 0.4. This qualitative argument can be formalized [50] to include more complicated configurations than shown in Fig. 3. On this basis, one can expect that replacing θ_d by θ with $a=1$ represents a suitable extension of the deposition probabilities of the WV model to continuous variables. This is confirmed by numerical integrations of the lattice Langevin equation for the 1D WV model [49,50], which quantitatively reproduce key properties of the WV model known from KMC simulations.

Equations (55) and (56), together with the expressions for the local deposition probabilities [49,99] and their extension to continuous variables [49,50], define the lattice Langevin equation for the 1D WV model. The calculation of local deposition probabilities can be automated [45,47,50] through symbolic manipulation, such as provided by MATHEMATICA [100]. This allows analogous derivations of lattice Langevin equations for which the transition rules resolve large numbers of height configurations. The lattice Langevin equation for the 1D WV model is then transformed into a continuum Langevin equation according to Sec. II. We can investigate the effect of a finite value of δ in the regularization (8) by comparing solutions of the Langevin equations to KMC simulations of the WV model. This comparison is based on the interface roughness $w(L,\tau)$ defined by

$$w(L,\tau) \equiv [\langle \mathbf{h}^2(\tau)\rangle - \langle \mathbf{h}(\tau)\rangle^2]^{1/2}, \tag{59}$$

where $\langle \mathbf{h}(\tau)^n\rangle = L^{-1}\Sigma_i h_i^n(t)$ for $n=1,2$, with an analogous definition for $\mathbf{H}(t)$. For sufficiently long times and large substrate sizes, w exhibits dynamic scaling [1]:

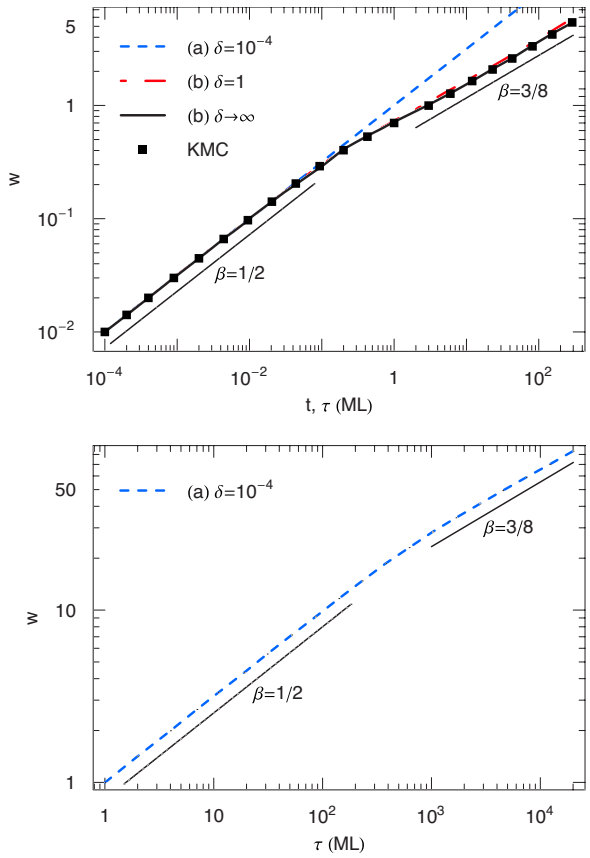

FIG. 4. (Color online) Roughness w defined in Eq. (59) versus time, measured in monolayers (ML) deposited, for the 1D WV model with $L=40\,000$ computed from KMC simulations and (a) the continuum Langevin equation (20) with the coefficients in Eqs. (67) and (68) (upper and lower panels) and (b) the 1D lattice Langevin equation (12) for the indicated values of δ (upper panel). Individual data sets were obtained from single realizations. Lines with slope $\beta=1/2$ and $\beta=3/8$, consistent with random deposition and the MH equation (23), respectively, are shown for comparison.

$$w(L,\tau) \sim L^{\alpha} f(\tau/L^z), \tag{60}$$

where the scaling function

$$f(x) \sim \begin{cases} x^{\beta} & \text{for } x \ll 1, \\ \text{constant} & \text{for } x \gg 1, \end{cases} \tag{61}$$

in which $\beta=\alpha/z$ is the growth exponent.

The top panel of Fig. 4 shows that for $\delta>1$ the interface roughness obtained from the lattice Langevin equation (12) and KMC simulations of the 1D WV model are in good agreement. This suggests that it is possible to obtain a corresponding large-order continuum equation that accurately describes the WV model, but we will not pursue this line of investigation here. As shown in the lower panel of Fig. 4, the coarse graining of height differences through Eq. (8) does not affect the scaling exponents, but delays the evolution of the Langevin equations, roughly by a factor of $1/(10\delta)$ for $\delta \ll 1$. In the random deposition regime, the Langevin equations yield excellent agreement with KMC simulations for

any $\delta > 0$ because in this regime the morphological evolution of the surface depends only on the deposition flux, which is independent of δ.

The leading-order equation (20) is obtained for the 1D WV model if the order of the dominant terms does not decrease as the coarse graining of height differences through Eq. (8) increases, which restricts δ to $\delta < \delta'$. As described in Sec. II, the value of δ', as well as the order of the continuum equation, is determined by comparing the maximum magnitudes of the coefficients at different orders in the spatial derivatives. Denoting the maximum magnitude of coefficients of terms of order n in the spatial derivatives by $\max[O(n)]$, we find for the 1D WV model that $\max[O(2)] \ll \max[O(4)]$ for any δ. As a result, the 1D WV model must be described by an equation involving at least second-order and fourth-order terms. We also find that

$$\max[O(4)] \gtrsim 3 \max[O(6)] \quad \text{for } \delta \lesssim 0.1,$$

$$\max[O(6)] \gtrsim 6 \max[O(8)] \quad \text{for } \delta \lesssim 0.07,$$

$$\max[O(8)] \gtrsim 10 \max[O(10)] \quad \text{for } \delta \lesssim 0.02,$$

which suggests $\delta \lesssim 0.02$ for the leading-order equation of the 1D WV model. Considering the slow decrease of higher-order corrections to the leading-order equation, as evidenced by the relatively large magnitudes of the coefficients of sixth-order and eighth-order terms, we use an upper bound of $\delta' = 0.001$. We will return to the motivation for this choice of δ' in Sec. IV B.

The signs and magnitudes of the coefficients in the leading-order equation for a given lattice model depend [46,47,50] on the physical parameters governing the transitions of the lattice model. The 1D WV model does not involve any such parameters and, hence, the coefficients in Eq. (20) only depend on the regularization parameter δ. For general $0 < \delta < \delta'$ we have

$$\nu_2 = B(\delta)\mathcal{P}_{-1,1}^2\mathcal{P}_{-2,4}, \tag{62}$$

$$\nu_4 = -\frac{1}{6}B(\delta)\mathcal{P}_{-19,64,-95,44}, \tag{63}$$

$$\lambda_{13} = B(\delta)^3\mathcal{P}_{2,-4} + B(\delta)C(\delta)\mathcal{P}_{8,-20,12} + D(\delta)\mathcal{P}_{1,-1}^2\mathcal{P}_{-2,4}, \tag{64}$$

$$\lambda_{22} = B(\delta)^2\mathcal{P}_{1,2,-4} + C(\delta)\mathcal{P}_{4,-10,16,-8}, \tag{65}$$

$D_0 = \tau_0/2$, and $D_2 = D_4 = 0$, where

$$\mathcal{P}_{l,m,n,\ldots} = l + mA(\delta) + nA(\delta)^2 + \cdots, \tag{66}$$

for simplicity we have set $a_\perp = a_\parallel = 1$, and $A(\delta)$, $B(\delta)$, $C(\delta)$, and $D(\delta)$ are the coefficients of the first four terms in the expansion of θ in Eq. (19) with $a = 1$.

For the representative choice $\delta = 10^{-4}$ the coefficients in Eqs. (62)–(65) evaluate to

$$\nu_2 = 2 \times 10^{-9}, \quad \nu_4 = 5 \times 10^{-5}, \tag{67}$$

$$\lambda_{13} = -4 \times 10^{-17}, \quad \lambda_{22} = 3 \times 10^{-9}, \tag{68}$$

from which we see that ν_4 is the dominant coefficient in the leading-order Langevin equation for the 1D WV model. As a result, the short-wavelength and high-frequency properties of this model are, to a good approximation, captured by the MH equation (23). This prediction is in excellent agreement with the initial behavior (up to the deposition of $\sim 10^5$ ML) observed in KMC simulations of the 1D WV model [51,54] and long-standing physical arguments [26,27] regarding the description of homoepitaxial surface growth. In the next section we will determine how the remaining terms in Eq. (20), which have coefficients with relatively small but finite values at atomistic scales, influence the behavior of the 1D WV model along the RG trajectory.

B. Renormalization-group trajectory

Figure 5 shows the RG trajectory of the 1D WV model, obtained by solving Eqs. (43)–(47) with the initial conditions in Eqs. (67) and (68). The RG flow exhibits a clear crossover from the MH to the VLDS fixed point, followed by a second crossover to the asymptotically stable EW fixed point. The crossover from the VLDS to the EW fixed point is influenced by a change in the magnitude of u_1. Although the term $\lambda_{13}\nabla(\nabla u)^3$ is often regarded as being negligible for lattice models of homoepitaxial growth [1], which is consistent with Eqs. (67) and (68) for the 1D WV model, its coarse-grained expression influences the morphological evolution. According to Fig. 5 the 1D WV model is described over expanding length and time scales by a hierarchy of linear and nonlinear continuum equations, given by the MH equation (23), the VLDS equation (24), and the EW equation (22). The fact that all terms in the continuum Langevin equation (20) have nonzero coefficients is a central property of the WV model and provides a critical test of our multiscale method.

The behavior of the WV model displayed in Fig. 5 is in excellent agreement with several KMC simulations [49,51,53,54], all of which find the same crossover sequence. Our analytic theory, however, also provides continuum equations for the crossover regimes, which are difficult to infer on the basis of computer simulations. The main features of the flow trajectory in Fig. 5 are independent of the choice for the parameter δ in the regularized step function, provided that $0 < \delta < \delta' \sim 0.001$, such that there is clear convergence towards the leading order continuum equation. If, on the other hand, $\delta > 0.001$, there is no crossover from the MH to the EW fixed point via the VLDS fixed point and the rescaled coefficients in Eqs. (38)–(40) diverge as $\ell \to \infty$. This is in disagreement with the results of the aforementioned KMC simulations. We conclude that for such values of δ higher-order terms need to be included in the RG analysis, which is also consistent with the considerations justifying the leading-order Langevin equation for the 1D WV model in Sec. IV A.

The trajectory in Fig. 5 shows that even a relatively simple lattice model can be governed by a sequence of differential equations, implying quite different behavior at different scales. It is therefore instructive to determine how "long" the 1D WV model is described by a given continuum equation. This necessitates defining a measure of "time" that

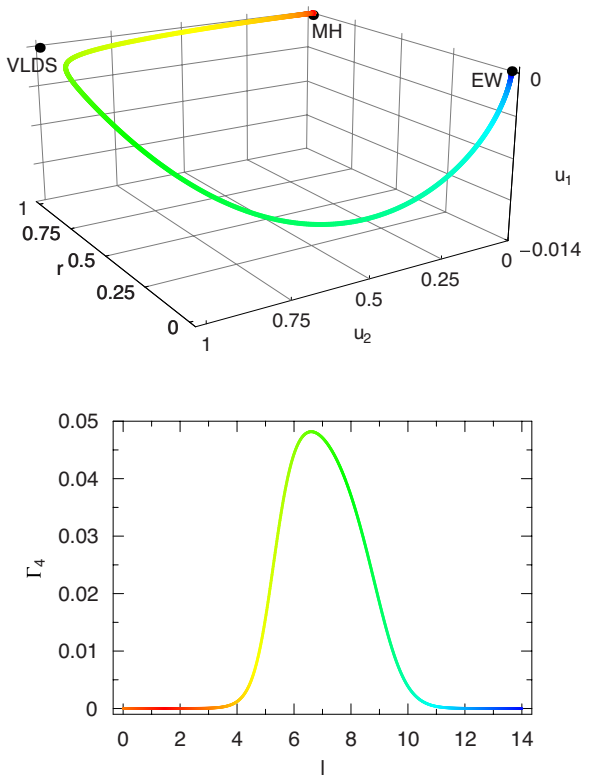

FIG. 5. (Color online) (top) RG trajectory of the 1D WV model obtained from Eqs. (43)–(47) with the initial conditions in Eqs. (67) and (68) and (bottom) the value of Γ_4 along the RG trajectory. The range of ℓ is the same in both panels, and $\Gamma_2=0$ along the RG trajectory.

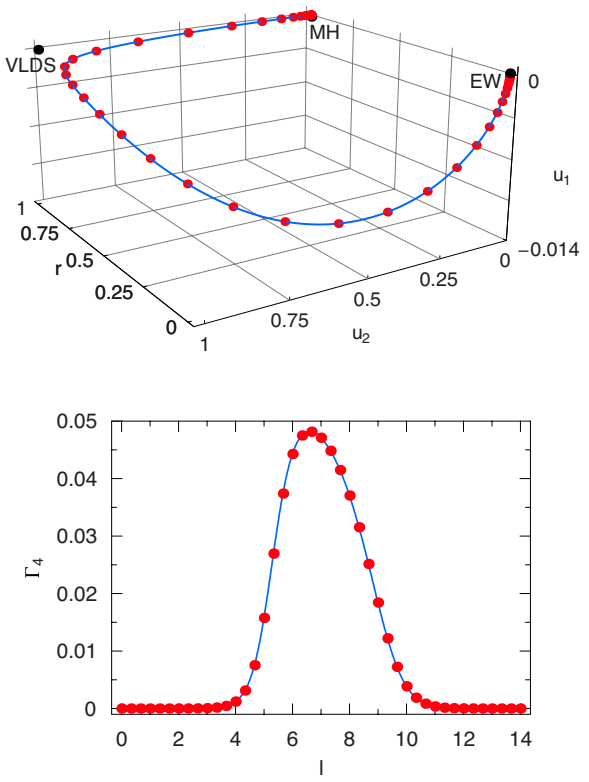

FIG. 6. (Color online) (top) RG trajectories of the 1D WV model and (bottom) of Γ_4 in Fig. 5. Superimposed on the trajectories are points separated by a logarithmic "scale" of $\Delta\ell=1/3$. The range of ℓ is the same in the upper and lower panels.

can be related to real systems. The time τ is only useful close to a given fixed point, in which case the scaling exponents are approximately constant. A more physically meaningful measure of crossover times is provided by the correlation length associated with each point along the RG trajectory [81]. On the other hand, if only a qualitative measure of the crossover time is required, it is sufficient to consider how rapidly the RG trajectory evolves as a function of the flow parameter ℓ. This is the approach we will adopt here, and the more accurate method based on the correlation length will be retained for future investigations.

Figure 6 shows the same trajectory as Fig. 5 with points superimposed on the trajectory that are spaced by a logarithmic "scale" $\Delta\ell=1/3$. We find that the flow near the VLDS fixed point is accelerated relative to the MH and EW fixed points, indicating a short residence time near the VLDS fixed point. The regions between these scaling regimes are crossed comparatively quickly. As noted above, close to a fixed point, values of $\Delta\ell$ can be related to time intervals $\Delta\tau$ through $\Delta\tau=e^{z\Delta\ell}$, with analogous expressions for Δx and Δu. For the MH fixed point we have $z=4$, for the VLDS fixed point $z=3$, and for the EW fixed point $z=2$ [1]. Thus, the evolution of the system is described by an extended MH regime, before crossing over briefly to a regime corresponding to the VLDS equation and finally approaching the EW fixed point. These relative crossover times are in excellent agreement with KMC simulations [49,54], in which τ is measured as the number of deposition events [101]. However, characterizing the final crossover of the 1D WV model to the EW fixed point requires quite extensive simulations [49,54], and an analytic theory is therefore useful in this case even from a purely computational perspective.

V. DISCUSSION

Sections II and III describe a general method for the multiscale analysis of stochastic lattice models. The RG analysis of Eq. (20) is generic and can be applied to a wide range of conservative lattice models satisfying basic symmetry constraints [1]. The fixed points of the transformed RG equations (43)–(47) in Table I exhaust the possible stable macroscopic limits of Eq. (20) under coarse gaining. In addition to the well-known EW, MH, and VLDS fixed points we also obtain the three previously unknown fixed points FP1, FP2, and FP3. It remains to be seen if any atomistic transition rules lead to RG trajectories approaching these new fixed points. The RG equations (26)–(32) open the door to a general characterization of the parameter space of systems described by Eq. (20). This will allow the partition of the space spanned by ν_2, ν_4, λ_{13}, λ_{22}, D_0, D_2, and D_4 into regions that are governed by a specified equation of motion at particular length and time scales. Thus, it becomes possible to systematically relate a coarse-grained equation to particular atomistic transition rules, which is the "inverse" question typically

addressed by computer simulations of lattice models.

Analytic RG transformations allow the derivation of equations describing the flow of the system under coarse graining. Such RG equations have the appealing feature of admitting a general analysis of parameter space, including the determination of possible macroscopic descriptions of the system in terms of fixed points. However, for complicated atomistic transition rules the corresponding leading-order Langevin equation can be considerably more complex than Eq. (20), making momentum-space RG transformations very cumbersome. Indeed, even for the 1D WV model, the continuum limit of the lattice Langevin equation is considerably more complex than Eq. (20) for $\delta > \delta_0$. Since the multiscale method discussed here does not rely on any particular implementation of the RG, coarse graining could also be applied in the spatial domain using methods based on the real-space RG. In addition to computational advantages, such an approach would also be especially suitable for inhomogeneous coarse graining [6,102]. This offers a systematic approach to concurrent multiscale modeling [6] that could, for example, lead to a first-principles derivation of the equations of the quasicontinuum method [103].

The most direct application of the RG equations (26)–(32) is to the coarse graining of lattice models describing epitaxial surface growth. But there are numerous other areas of research that could benefit from an analysis analogous to that presented here. Previous work [56,57] suggests that potentially a wide variety of lattice models are amenable to the basic approach outlined in this paper. For example, our method could be used to derive a continuum theory for lattice models of self-organized criticality [104–106]. Indeed, continuum equations have been proposed for self-organized criticality generally based on phenomenological arguments [105–107] and a direct connection has been made [108] between the Oslo rice pile model and the quenched EW model. The application of our method to such models could address issues that are similar to those for growth models, such as the robustness to changes of their rules and the direct calculation of critical quantities associated with the self-organized state. Thus, at least in principle, it would be possible to calculate RG trajectories, thereby revealing the behavior of such systems for any length and time scales. This would also allow the systematic classification of model systems for self-organized criticality into universality classes, which remains a subject of great interest [105–108].

Another area in which our method could find fruitful applications is fluid dynamics. Much effort has been devoted in this field to establishing direct relationships between lattice gas models and continuum equations [4,5]. Indeed, for the simple case of the one-dimensional asymmetric exclusion process the derivation of lattice and continuum Langevin equations yields, consistent with previous studies, Burgers' equation as a deterministic description [56]. Motivated by the study of randomly stirred fluids, stochastic forms of Burgers' equation have been successfully analyzed with RG methods [80]. This suggests that an approach similar to that taken in this paper could be suitable for lattice gases of fluid dynamics. Apart from insights into particular aspects of fluid dynamics, such applications would also lead to a further generalization of the methods used in this paper.

Finally, our multiscale method suggests a number of mathematical questions. The transformation from discrete to continuous height and time variables can, in principle, be given a firm mathematical foundation on the basis of limit theorems due to Kurtz [60–68]. In practice, however, this generally necessitates a nontrivial extension of the transition rules to noninteger variables. While plausible from a physical perspective, the procedure used here lacks mathematical rigor. Similarly, the passage to the continuum limit that has been carried out in this paper, although systematic and convergent, does not have a formal mathematical justification. This problem originates with the step functions, which are artifacts of our use of lattice models whose transition rules necessitate counting relative heights at neighboring sites. While convenient from a computational perspective, the singular nature of the step functions hinders the further analysis of such models. Nevertheless, despite such open mathematical questions, the calculations presented here and in Refs. [45–47,50,56,57,71,72] suggest that the method described in this paper provides a versatile basis for investigating the coarse-grained expression of atomistic rules in many settings.

VI. SUMMARY AND CONCLUSIONS

We have described a general framework for the multiscale analysis of stochastic lattice models. Our method consists of two basic steps. In the first step (Sec. II), lattice Langevin equations are derived which embody the transition rules of lattice models. As discussed in greater detail in Ref. [49], these lattice Langevin equations constitute an analytic adjunct to KMC simulations and could be used, for instance, to lend analytic support to acceleration methods employed in such simulations. The continuum equations corresponding to the lattice equations are obtained by regularizing the atomistic transition rules. Depending on the regularization, either a large-order equation is obtained that can capture essentially all properties of the lattice equations or a low-order equation that describes only fundamental properties such as the scaling behavior. While the investigation of large-order continuum equations is not feasible with the analytic methods used in this paper, numerical methods might be better equipped to deal with the complicated structure of these equations.

In the second step of our method (Sec. III), the coefficients in the (leading-order) regularized Langevin equation serve as initial conditions for RG transformations. The RG trajectories of the coefficients correspond to hierarchies of continuum equations describing lattice models over expanding length and time scales. This provides a systematic method for the derivation of continuum equations from the transition rules of lattice models for any length and time scales. We have illustrated this procedure (Sec. IV) for the 1D WV model. In this case the coarse graining of the leading-order Langevin equation gives a hierarchy of continuum equations characterized by a crossover from the MH equation (23) to the VLDS equation (24), followed by a final crossover to the EW equation (22), which is in excellent agreement with KMC simulations [49,51,53,54]. Similarly

complex crossover sequences are obtained [45–47,50] for other models of surface growth and are also found to be in agreement with KMC simulations. This suggests that our method provides a suitable framework for the multiscale analysis of general nonequilibrium systems described by stochastic lattice models.

ACKNOWLEDGMENTS

This work was supported by funds from the U.K. Engineering and Physical Sciences Research Council and the European Commission Sixth Framework Programme as part of the European Science Foundation EUROCORES Programme on Self-Organized Nanostructures (SONS).

APPENDIX A: DIAGRAMMATIC RENORMALIZATION-GROUP CALCULATION

This appendix provides a detailed description of the RG analysis of the continuum Langevin equation (20) in terms of the diagrammatic formulation of the dynamic RG [22,23,77,78,80]. Since we use a momentum-space implementation of the dynamic RG, it will first be necessary to transform Eqs. (20) and (21) into Fourier space. Subsequently, contributions to the evolution of the system associated with small length and time scales are absorbed into a redefinition of the coefficients in the Langevin equation, which completes the first step of the RG. This is achieved through a formal perturbation expansion of the Langevin equation combined with a regularization of the integrals. In the second and final step of the RG the spatial variable is rescaled to its original range, with a corresponding rescaling of all other physical quantities. The outcome of this procedure is a system of ordinary differential equations describing the modification of the coefficients in Eqs. (20) and (21) under repeated coarse graining and rescaling.

1. Fourier transformation of the Langevin equation

We use the following Fourier transforms of $u(\mathbf{x},\tau)$ and $\xi(\mathbf{x},\tau)$:

$$u(\mathbf{x},\tau) = \int \frac{d\mathbf{k}}{(2\pi)^d} \int \frac{d\omega}{2\pi} e^{i(\mathbf{k}\cdot\mathbf{x}-\omega\tau)} u(\mathbf{k},\omega), \tag{A1}$$

$$\xi(\mathbf{x},\tau) = \int \frac{d\mathbf{k}}{(2\pi)^d} \int \frac{d\omega}{2\pi} e^{i(\mathbf{k}\cdot\mathbf{x}-\omega\tau)} \xi(\mathbf{k},\omega). \tag{A2}$$

Defining the *bare propagator* $G_0(\mathbf{k},\omega)$ by [23,77,80]

$$G_0(\mathbf{k},\omega) \equiv \frac{1}{\nu_2 k^2 + \nu_4 k^4 - i\omega}, \tag{A3}$$

we can rewrite Eq. (20) in Fourier space as

$$u(\mathbf{k},\omega) = G_0(\mathbf{k},\omega)\xi(\mathbf{k},\omega) + \lambda_{22} G_0(\mathbf{k},\omega) k^2 \int \frac{d\mathbf{q}}{(2\pi)^d} \int \frac{d\Omega}{2\pi} \times [\mathbf{q}\cdot(\mathbf{k}-\mathbf{q})] u(\mathbf{k}-\mathbf{q},\omega-\Omega) u(\mathbf{q},\Omega) + \lambda_{13} G_0(\mathbf{k},\omega) \times \int \frac{d\mathbf{q}'}{(2\pi)^d} \int \frac{d\mathbf{q}''}{(2\pi)^d} \int \frac{d\Omega'}{2\pi} \int \frac{d\Omega''}{2\pi} [\mathbf{k}\cdot(\mathbf{k}-\mathbf{q}')] \times [\mathbf{q}''\cdot(\mathbf{q}'-\mathbf{q}'')] u(\mathbf{k}-\mathbf{q}',\omega-\Omega') \times u(\mathbf{q}'',\Omega'') u(\mathbf{q}'-\mathbf{q}'',\Omega-\Omega''), \tag{A4}$$

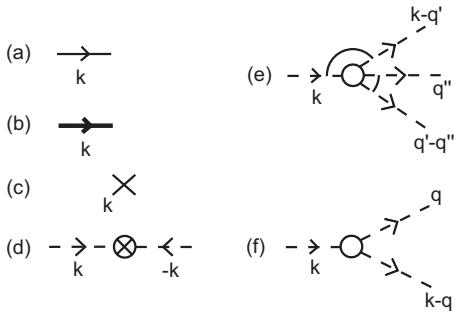

FIG. 7. Feynman rules for Eq. (A4). The corresponding mathematical expressions of different diagrammatic elements are (a) $G_0(\mathbf{k},\omega)$, (b) $G(\mathbf{k},\omega)$, (c) $\xi(\mathbf{k},\omega)$, (d) 2 $(D_0+k^2D_2+k^4D_4)$, (e) λ_{13} $[\mathbf{k}\cdot(\mathbf{k}-\mathbf{q}')][\mathbf{q}''\cdot(\mathbf{q}'-\mathbf{q}'')]$, and (f) $\lambda_{22}k^2$ $[\mathbf{q}\cdot(\mathbf{k}-\mathbf{q})]$. Equations (A4) and (A5) mandate that at each vertex the input momenta and frequencies equal the output momenta and frequencies and that at each noise contraction the input momenta and frequencies sum to zero. Integrals of the form $\int[d\mathbf{q}/(2\pi)^d]\int(d\Omega/2\pi)$ are associated with all internal momentum and frequency variables.

where $\xi(\mathbf{k},\omega)$ is Gaussian noise with zero mean and, for D_2=const, covariance [50]

$$\langle \xi(\mathbf{k},\omega)\xi(\mathbf{k}',\omega')\rangle = 2(2\pi)^{d+1}\mathcal{D}_F\delta(\mathbf{k}+\mathbf{k}')\delta(\omega+\omega'), \tag{A5}$$

in which $\mathcal{D}_F = D_0 + D_2\mathbf{k}^2$. The form of the above expressions can be confirmed by dimensional analysis [50].

2. Intermediate flow equations

In the diagrammatic implementation of the dynamic RG, Eq. (A4) is the starting point for a formal iterative calculation of u in powers of λ_{22} and λ_{13} using a diagrammatic representation of the momentum-space Langevin equation. The appropriate Feynman rules are formulated in analogy to those in Refs. [22,23,80] and summarized in Fig. 7. The effective propagator $G(\mathbf{k},\omega)$ is defined as [23]

$$u(\mathbf{k},\omega) \equiv G(\mathbf{k},\omega)\xi(\mathbf{k},\omega), \tag{A6}$$

which is the generalization of the bare propagator in Eq. (A3) to the full equation (A4) including linear *and* nonlinear terms. Moreover, for reasons which will be discussed below, we have modified the noise covariance in Eq. (A5) to $\mathcal{D}_F = D_0 + D_2k^2 + D_4k^4$, where D_4 is a constant. Using these rules, Eq. (A4) can be represented as shown in Fig. 8.

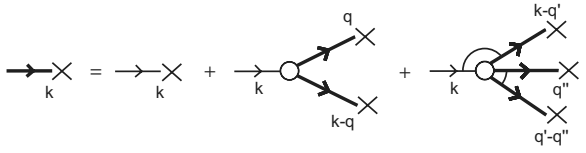

FIG. 8. Graphic representation of the integral equation (A4) according to the Feynman rules in Fig. 7.

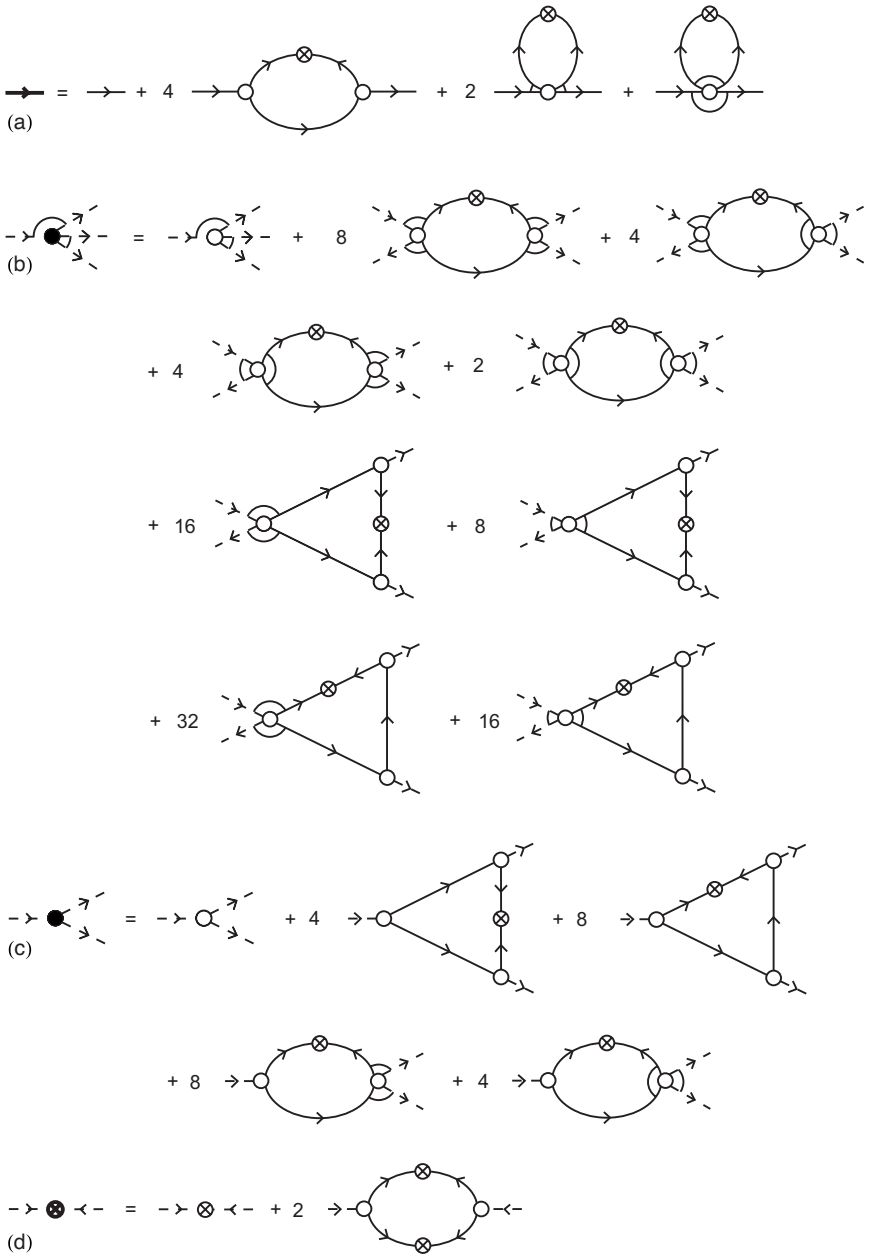

FIG. 9. Intermediate one-loop flow equations for (a) the propagator G, (b) the λ_{13} vertex, (c) the λ_{22} vertex, and (d) the noise covariance $\mathcal{D}_F$. We label the one-loop corrections to the propagator $\Phi_1-\Phi_3$, to the λ_{13} vertex $\Xi_1-\Xi_8$, to the λ_{22} vertex $\Gamma_1-\Gamma_4$, and to the noise covariance Δ, respectively.

In the first step of the dynamic RG [80,77], the equation of motion is projected onto the phase space spanned by the modes with $0<k<e^{-d\ell}\Lambda$, where $d\ell$ denotes an infinitesimal positive change in the flow parameter ℓ and the cutoff Λ is associated with a minimum length scale $2\pi\Lambda^{-1}$. The projection of the equation of motion is achieved [77] by splitting the function $u(\mathbf{k},\omega)$ into fast modes $u^>$ for which $e^{-d\ell}\Lambda<k<\Lambda$ and slow modes $u^<$ for which $0<k<e^{-d\ell}\Lambda$. The equation for $u^>$ is then solved iteratively in terms of $u^<$ up to some prescribed order, and this expression for $u^>$ is substituted into the equation for $u^<$. Finally, $u^<$ is averaged over the part of the noise that acts in the shell $e^{-d\ell}\Lambda<k<\Lambda$ such that all dependence on short-wavelength modes is removed [90]. By absorbing all contributions due to $u^>$ into redefinitions of the coefficients appearing in the Langevin equation, one thus obtains an "effective" equation for $u^<$, with modified coefficients and, possibly, more terms than in the original equation for u, but with the same symmetry. In practice, this procedure amounts to [80] a formal iterative calculation of u, with the interpretation that external lines correspond to $u^<$, and internal lines to $u^>$.

The intermediate flow equations for Eq. (A4) are given to one-loop order in Fig. 9. The symbols on the left-hand side denote *effective* graphs, which obey the Feynman rules in Fig. 7, but with the set of coefficients $(\nu_2,\nu_4,\lambda_{13},\lambda_{22},\mathcal{D}_F)$ replaced by the effective coefficients $(\nu_2^<,\nu_4^<,\lambda_{13}^<,\lambda_{22}^<,\mathcal{D}_F^<)$ associated with the equation for $u^<$. In analogy to the bare propagator G_0 one writes the *effective propagator* [91] G as [23]

$$G(\mathbf{k},\omega)=\frac{1}{\nu_2^<k^2+\nu_4^<k^4-i\omega} \tag{A7}$$

for $0<k<e^{-d\ell}\Lambda$. The averaging over noise in the range $e^{-d\ell}\Lambda<k<\Lambda$ means that the loop integrations in Fig. 9 are

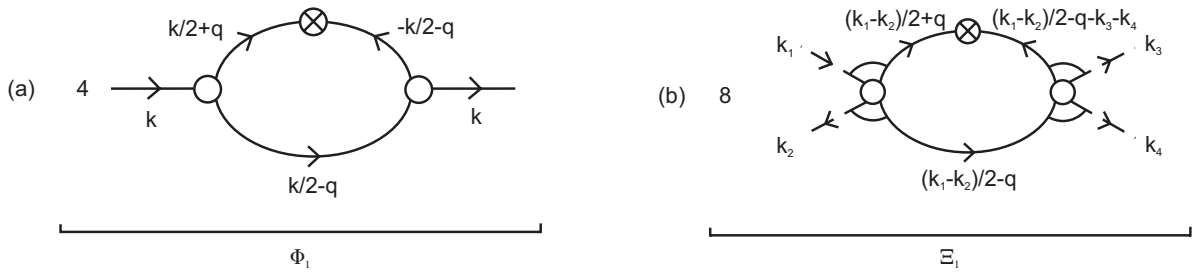

FIG. 10. Feynman graphs for sample calculations: (a) the first graph in the equation for G in Fig. 9 and (b) the first graph in the equation for $\lambda_{13}^{<}$ in Fig. 9. The external momentum k in graph (a) is split equally between internal lines to allow the simultaneous evaluation of the four graphs generated by the diagrammatic expansion [50].

restricted to the shell $e^{-d\ell}\Lambda<k<\Lambda$. External lines in these equations carry momenta in the range $0<k<e^{-d\ell}\Lambda$, and internal lines carry momenta with $e^{-d\ell}\Lambda<k<\Lambda$ [77,80]. Finally, we note that the reorganization of the expansion for $u^{<}$ as an expansion for the coefficients means that only one-particle irreducible graphs, which cannot be split by cutting a single line, must be considered.

Apart from the intermediate flow equations for the deterministic part of the equation of motion (A4), given by the equations for $G^{<}$, $\lambda_{13}^{<}$, and $\lambda_{22}^{<}$, Fig. 9 also shows the equation for the effective noise covariance $\mathcal{D}_F^{<}=D_0^{<}+k^2D_2^{<}+k^4D_4^{<}$. The equation for $\mathcal{D}_F^{<}$ follows directly from Eq. (A6) and is given by [23]

$$\langle u^{<}(\mathbf{k},\omega)u^{<}(-\mathbf{k},-\omega)\rangle = 2\mathcal{D}_F^{<}G(\mathbf{k},\omega)G(-\mathbf{k},-\omega), \tag{A8}$$

where the right-hand side of the equation for $\mathcal{D}_F^{<}$ in Fig. 9 is obtained by evaluating the left-hand side of Eq. (A8) using Eq. (A6). In particular, the Feynman rules in Fig. 7 imply that the one-loop contribution to $\mathcal{D}_F^{<}$ is of $O(k^4)$. As a result, the term $D_4\nabla^4$ is generated as the leading-order correction to the noise covariance $\mathcal{D}$ even though $D_4=0$ in Eq. (21). For simplicity we have therefore already included this term in the definition of the Feynman rules above.

3. Evaluation of Feynman graphs

This section illustrates the evaluation of the Feynman graphs in Fig. 9 through two representative calculations. The evaluation of all remaining graphs is described in detail in Ref. [50]. We will consider the one-loop corrections to G and $\lambda_{13}^{<}$ displayed in Fig. 10. The internal variables are thereby chosen to simplify the evaluation of the graphs and to allow direct comparisons with previous RG calculations [22–24,29] of related problems. For future reference we also define

$$\nu(\mathbf{q}) = \nu_2 + \nu_4\mathbf{q}^2, \quad \mathcal{D}_F(\mathbf{q}) = D_0 + D_2\mathbf{q}^2 + D_4\mathbf{q}^4,$$

$$D_s(\mathbf{q}) = \sum_{i=0}^{2} [(d-4+2i)\nu(\mathbf{q}) - 2\nu_4\mathbf{q}^2]D_{2i}\mathbf{q}^{2i}, \tag{A9}$$

with $\nu=\nu(\Lambda)$, $D=\mathcal{D}_F(\Lambda)$, and $D_s=D_s(\Lambda)$.

According to the Feynman rules in Fig. 7, the graph Φ_1 is given by

$$\Phi_1 = 4\lambda_{22}^2\int^{q>}\frac{d\mathbf{q}}{(2\pi)^d}\int_{-\infty}^{\infty}\frac{d\Omega}{2\pi}2\mathcal{D}_F\left(\frac{\mathbf{k}}{2}+\mathbf{q}\right)$$
$$\times\mathbf{k}^2\left[\left(\frac{\mathbf{k}}{2}+\mathbf{q}\right)\cdot\left(\frac{\mathbf{k}}{2}-\mathbf{q}\right)\right]\left[-\left(\frac{\mathbf{k}}{2}+\mathbf{q}\right)\cdot\mathbf{k}\right]\left[\left(\frac{\mathbf{k}}{2}-\mathbf{q}\right)^2\right]$$
$$\times G_0\left(\frac{\mathbf{k}}{2}+\mathbf{q},\frac{\omega}{2}+\Omega\right)G_0\left(\frac{\mathbf{k}}{2}-\mathbf{q},\frac{\omega}{2}-\Omega\right)$$
$$\times G_0\left(-\frac{\mathbf{k}}{2}-\mathbf{q},-\frac{\omega}{2}-\Omega\right), \tag{A10}$$

where the momentum integration is over the spherical shell $e^{-d\ell}\Lambda<q<\Lambda$ since at this stage of the RG procedure we have already averaged over short-wavelength modes and for simplicity we have omitted the external bare propagators $G_0(\mathbf{k},\omega)$.

To evaluate this graph we transform the momentum integral to spherical polar coordinates and obtain

$$\Phi_1 = 4\lambda_{22}^2k^2\int_{-\infty}^{\infty}\frac{d\Omega}{\pi}\frac{S_{d-1}}{(2\pi)^d}\int_0^{\pi}d\theta\sin^{d-2}\theta\int^{q>}dqq^{d-1}$$
$$\times\mathcal{D}_F\left(\frac{\mathbf{k}}{2}+\mathbf{q}\right)\left(-q^2+\frac{k^2}{4}\right)\left(-kq\cos\theta-\frac{k^2}{2}\right)$$
$$\times\left(q^2-kq\cos\theta+\frac{k^2}{4}\right)G_0\left(\frac{\mathbf{k}}{2}+\mathbf{q},\omega+\Omega\right)$$
$$\times G_0\left(\frac{\mathbf{k}}{2}-\mathbf{q},\frac{\omega}{2}-\Omega\right)G_0\left(-\frac{\mathbf{k}}{2}-\mathbf{q},-\frac{\omega}{2}-\Omega\right), \tag{A11}$$

where S_{d-1} is the surface area of a $(d-1)$-dimensional unit sphere. Since by convention the coefficient of u_τ does not change under RG transformations, we are free to set $\omega=0$ in the above expression without loss of generality.

We now transform the dummy variable in the frequency integral to $z=\Omega/(\nu_2q^2+\nu_4q^4)$ and obtain the leading-order contribution in k due to this graph by expanding the bare propagators with respect to k around $k=0$, keeping terms up to $O(k^4)$. The evaluation of the Ω and θ integrals then reduces to the evaluation of the integrals

$$\int_{-\infty}^{\infty}\frac{dz}{\pi}\frac{1}{(1-iz)(1+iz)^2} = \frac{1}{2},$$

$$K_d = \frac{S_{d-1}}{(2\pi)^d}\int_0^\pi d\theta \sin^{d-2}\theta = \frac{S_d}{(2\pi)^d},$$

$$\frac{S_{d-1}}{(2\pi)^d}\int_0^\pi d\theta \sin^{d-2}\theta \cos^2\theta = \frac{K_d}{d}. \tag{A12}$$

Using the above results we obtain

$$\Phi_1 = k^4 \frac{K_d}{d}\lambda_{22}^2 \int^{q^>} dq q^{d-1} \frac{D_s(q)}{\nu(q)^3} \tag{A13}$$

to leading order in k. Carrying out a Taylor expansion of the integrand around $q=\Lambda$, and keeping terms only to $O(d\ell)$, we find

$$\Phi_1 = k^4 \frac{K_d}{d}\frac{\lambda_{22}^2 D_s \Lambda^d}{\nu^3} d\ell. \tag{A14}$$

Since this expression is $O(k^4)$, we conclude that the graph Φ_1 produces a correction to ν_4.

According to the Feynman rules in Fig. 7 the graph Ξ_1 is given by

$$\begin{aligned}\Xi_1 = 8\lambda_{13}^2 \int^{q^>} \frac{d\mathbf{q}}{(2\pi)^d}\int_{-\infty}^{\infty}\frac{d\Omega}{2\pi} 2\mathcal{D}_F\left(\frac{\mathbf{k}_1-\mathbf{k}_2}{2}+\mathbf{q}\right)\\ \times\left[\mathbf{k}_1\cdot\left(\frac{\mathbf{k}_1-\mathbf{k}_2}{2}+\mathbf{q}\right)\right]\left[\mathbf{k}_2\cdot\left(\frac{\mathbf{k}_1-\mathbf{k}_2}{2}-\mathbf{q}\right)\right]\\ \times\left[\mathbf{k}_4\cdot\left(\frac{\mathbf{k}_1-\mathbf{k}_2}{2}-\mathbf{q}\right)\right]\left[\mathbf{k}_3\cdot\left(\frac{\mathbf{k}_1-\mathbf{k}_2}{2}-\mathbf{q}-\mathbf{k}_3-\mathbf{k}_4\right)\right]\\ \times G_0\left(\frac{\mathbf{k}_1-\mathbf{k}_2}{2}+\mathbf{q},\frac{\omega_1-\omega_2}{2}+\Omega\right)\\ \times G_0\left(\frac{\mathbf{k}_1-\mathbf{k}_2}{2}-\mathbf{q},\frac{\omega_1-\omega_2}{2}-\Omega\right)\\ \times G_0\left(\frac{\mathbf{k}_1-\mathbf{k}_2}{2}-\mathbf{q}-\mathbf{k}_3-\mathbf{k}_4,\frac{\omega_1-\omega_2}{2}-\Omega-\omega_3-\omega_4\right),\end{aligned} \tag{A15}$$

where the momentum integration is over the spherical shell $e^{-d\ell}\Lambda < q < \Lambda$.

As for Φ_1, we evaluate Ξ_1 by transforming the momentum integral to spherical coordinates and replacing the dummy variable in the frequency integral by $z=\Omega/(\nu_2 q^2+\nu_4 q^4)$. To leading order in k the momentum contractions yield

$$-(\mathbf{k}_1\cdot\mathbf{q})(\mathbf{k}_2\cdot\mathbf{q})(\mathbf{k}_3\cdot\mathbf{q})(\mathbf{k}_4\cdot\mathbf{q}). \tag{A16}$$

Since this expression is already $O(k^4)$, we need only expand the noise covariance as $\mathcal{D}_F \propto 1+O(k)$, and the bare propagators as $G_0 \propto 1+O(k)$ to obtain

$$\begin{aligned}\Xi_1 = -8\lambda_{13}^2 \int_{-\infty}^{\infty}\frac{dz}{\pi}\int\frac{dS}{(2\pi)^d}\int^{q^>} dq q^{d-1}(\nu_2 q^2+\nu_4 q^4)\mathcal{D}_F(q)\\ \times(\mathbf{k}_1\cdot\mathbf{q})(\mathbf{k}_2\cdot\mathbf{q})(\mathbf{k}_3\cdot\mathbf{q})(\mathbf{k}_4\cdot\mathbf{q})\\ \times\frac{1}{(1-iz)(1+iz)^2}\left(\frac{1}{\nu_2 q^2+\nu_4 q^4}\right)^3,\end{aligned} \tag{A17}$$

where the angular integral $\int dS$ is to be taken over the complete spherical shell and, as for Φ_1, we have set $\omega=0$.

To evaluate the above expression for Ξ_1 we note that [50]

$$\begin{aligned}\int^{q^>} dq q^{d-1}\int\frac{dS}{(2\pi)^d}(\mathbf{a}\cdot\mathbf{q})(\mathbf{b}\cdot\mathbf{q})(\mathbf{c}\cdot\mathbf{q})(\mathbf{d}\cdot\mathbf{q})\\ = \frac{K_d}{d(d+2)}[(\mathbf{a}\cdot\mathbf{b})(\mathbf{c}\cdot\mathbf{d})+(\mathbf{a}\cdot\mathbf{c})(\mathbf{b}\cdot\mathbf{d})\\ +(\mathbf{a}\cdot\mathbf{d})(\mathbf{b}\cdot\mathbf{c})]\int^{q^>} dq q^{d-1}q^4,\end{aligned} \tag{A18}$$

where $\mathbf{a}$, $\mathbf{b}$, $\mathbf{c}$, and $\mathbf{d}$ are arbitrary constant vectors. Thus, we obtain

$$\begin{aligned}\Xi_1 = -8\lambda_{13}^2\frac{1}{2}\frac{K_d}{d(d+2)}\int^{q^>} dq q^{d-1}\left(\frac{1}{\nu_2 q^2+\nu_4 q^4}\right)^2 q^4\mathcal{D}_F(q)\\ \times[(\mathbf{k}_1\cdot\mathbf{k}_2)(\mathbf{k}_3\cdot\mathbf{k}_4)+(\mathbf{k}_1\cdot\mathbf{k}_3)(\mathbf{k}_2\cdot\mathbf{k}_4)\\ +(\mathbf{k}_1\cdot\mathbf{k}_4)(\mathbf{k}_2\cdot\mathbf{k}_3)].\end{aligned} \tag{A19}$$

Carrying out a Taylor expansion of the integrand around $q=\Lambda$, evaluating the q integral, and keeping terms only to $O(d\ell)$ we therefore find

$$\begin{aligned}\Xi_1 = -8\lambda_{13}^2 D\Lambda^d\frac{1}{2}\frac{K_d}{d(d+2)}\frac{d\ell}{\nu^2}[(\mathbf{k}_1\cdot\mathbf{k}_2)(\mathbf{k}_3\cdot\mathbf{k}_4)\\ +(\mathbf{k}_1\cdot\mathbf{k}_3)(\mathbf{k}_2\cdot\mathbf{k}_4)+(\mathbf{k}_1\cdot\mathbf{k}_4)(\mathbf{k}_2\cdot\mathbf{k}_3)].\end{aligned} \tag{A20}$$

The different dot products in the above expression for Ξ_1 correspond to different choices for the momentum contractions in the λ_{13} vertex. They appear because the choice of output leg to be contracted with the input leg is arbitrary. However, upon inverting the Fourier transformations all three of these contractions correspond to an identical term in the equation of motion. The three intermediate flow equations implied by Eq. (A20) therefore all contribute to the flow equation for λ_{13} and yield an overall correction of

$$\Xi_1 = -4\frac{3K_d}{d(d+2)}\frac{D\lambda_{13}^2\Lambda^d}{\nu^2}d\ell, \tag{A21}$$

where we have divided out the external momenta.

The calculation of the remaining graphs in Fig. 9 is analogous to the evaluation of Φ_1 and Ξ_1 and does not introduce any further complications. The result of the complete calculation [50] of the intermediate RG flow equations in Fig. 9 is summarized in Table II. Note, in particular, that graph Ξ_5 cancels Ξ_7 and that graph Ξ_6 cancels Ξ_8. Hence, the vertex λ_{13} is not renormalized by the vertex λ_{22}. In addition, Γ_1 is found to cancel Γ_2, which is consistent with previous calculations [24,25,29]. Also note that Ξ_2 and Ξ_3 give identical contributions, as expected on symmetry grounds.

TABLE II. One-loop corrections to G, λ_{13}, λ_{22}, and $\mathcal{D}_F$ calculated from the intermediate flow equations displayed in Fig. 9. For simplicity all external momenta have been divided out.

$$\Phi_1=\frac{K_d}{d}\frac{D_s\lambda_{22}^2\Lambda^d}{\nu^3}d\ell \qquad \Phi_2=-2\frac{K_d}{d}\frac{D\lambda_{13}\Lambda^d}{\nu}d\ell \qquad \Phi_3=-K_d\frac{D\lambda_{13}\Lambda^d}{\nu}d\ell$$

$$\Xi_1=-4\frac{3K_d}{d(d+2)}\frac{\lambda_{13}^2D\Lambda^d}{\nu^2}d\ell \qquad \Xi_2=\Xi_3=-2\frac{K_d}{d}\frac{\lambda_{13}^2D\Lambda^d}{\nu^2}d\ell \qquad \Xi_4=-K_d\frac{\lambda_{13}^2D\Lambda^d}{\nu^2}d\ell$$

$$\Xi_5=8\frac{3K_d}{d(d+2)}\frac{\lambda_{22}^2\lambda_{13}D\Lambda^{d+2}}{\nu^3}d\ell \qquad \Xi_6=4\frac{K_d}{d}\frac{\lambda_{22}^2\lambda_{13}D\Lambda^{d+2}}{\nu^3}d\ell \qquad \Xi_7=-8\frac{3K_d}{d(d+2)}\frac{\lambda_{22}^2\lambda_{13}D\Lambda^{d+2}}{\nu^3}d\ell$$

$$\Xi_8=-4\frac{K_d}{d}\frac{\lambda_{22}^2\lambda_{13}D\Lambda^{d+2}}{\nu^3}d\ell \qquad \Gamma_1=2\frac{K_d}{d}\frac{\lambda_{22}^3D\Lambda^{d+2}}{\nu^3}d\ell \qquad \Gamma_2=-2\frac{K_d}{d}\frac{\lambda_{22}^3D\Lambda^{d+2}}{\nu^3}d\ell$$

$$\Gamma_3=-4\frac{K_d}{d}\frac{\lambda_{22}\lambda_{13}D\Lambda^d}{\nu^2}d\ell \qquad \Gamma_4=-2K_d\frac{\lambda_{22}\lambda_{13}D\Lambda^d}{\nu^2}d\ell \qquad \Delta=2K_d\frac{\lambda_{22}^2D^2\Lambda^{d-2}}{\nu^3}d\ell$$

4. Rescaling

In the second step of the dynamic RG the spatial variable appearing in the effective equation of motion is rescaled to its original range, with a corresponding rescaling of all other physical quantities. For this purpose, first note that under the change of scale $\mathbf{x}\to e^{d\ell}\mathbf{x}$, $\tau\to e^{zd\ell}\tau$, and $u\to e^{\alpha d\ell}u$ the equation of motion (20) scales as

$$\frac{\partial u}{\partial\tau}=e^{(z-2)d\ell}\nu_2\nabla^2u-e^{(z-4)d\ell}\nu_4\nabla^4u+e^{(2\alpha+z-4)d\ell}\lambda_{13}\nabla(\nabla u)^3+e^{(\alpha+z-4)d\ell}\lambda_{22}\nabla^2(\nabla u)^2+e^{(z/2-d/2-\alpha)d\ell}\xi, \tag{A22}$$

where, by convention, the coefficient of u_τ is kept fixed at unity and for simplicity we have only considered at this stage the scaling of the nonconserved part of the noise term.

The intermediate one-loop flow equation for the propagator represented in the first line of Fig. 9 translates into standard mathematics as follows:

$$G(\mathbf{k},0)=G_0(\mathbf{k},0)[1+G_0(\mathbf{k},0)(\Phi_1+\Phi_2+\Phi_3)]. \tag{A23}$$

Inverting Eq. (A35) and dividing by k^2 we find

$$\nu_2^<+\nu_4^<k^2=(\nu_2+\nu_4k^2)[1+G_0(\mathbf{k},0)(\Phi_1+\Phi_2+\Phi_3)]^{-1}, \tag{A24}$$

where we have set $\omega=0$ because, as noted above, the coefficient of u_τ is kept fixed at unity. Expanding the fraction around $d\ell=0$ and keeping terms up to $O(d\ell)$ only one obtains

$$\nu_2^<+\nu_4^<k^2=\nu_2+\frac{K_d(d+2)}{d}\frac{\lambda_{13}D\Lambda^d}{\nu}d\ell+k^2\left\{\nu_4-\frac{K_d}{d}\frac{\lambda_{22}^2D_s\Lambda^d}{\nu^3}d\ell\right\}. \tag{A25}$$

For infinitesimal scale transformations the effective parameter $\nu_2^<$ is therefore related to the renormalized parameter $\tilde{\nu}_2$ through

$$\tilde{\nu}_2=e^{(z-2)d\ell}\nu_2^<\approx[1+(z-2)d\ell]\nu_2^<=[1+(z-2)d\ell]\nu_2\left\{1+\frac{K_d(d+2)}{d}\frac{\lambda_{13}D\Lambda^d}{\nu_2\nu}d\ell\right\} \tag{A26}$$

to one-loop order and, similarly, $\nu_4^<$ is related to $\tilde{\nu}_4$ via

$$\tilde{\nu}_4=e^{(z-4)d\ell}\nu_4^<\approx[1+(z-4)d\ell]\nu_4^<=[1+(z-4)d\ell]\nu_4\left\{1-\frac{K_d}{d}\frac{\lambda_{22}^2D_s\Lambda^d}{\nu_4\nu^3}d\ell\right\}. \tag{A27}$$

Equations (A26) and (A27) directly reflect the two steps of the dynamic RG. The first step yields expressions for $\nu_2^<$ and $\nu_4^<$, which are the effective ν_2 and ν_4 obtained after integrating out and averaging over small-wavelength degrees of freedom. In the second step, the quantities in terms of which the description of the system is cast are rescaled such that basic physical parameters in the "new" system, such as the lattice spacing $2\pi/\Lambda$, take the same value as in the "old" system. This defines the renormalized quantities $\tilde{\nu}_2$ and $\tilde{\nu}_4$.

Taking $d\ell\to0$ we finally obtain the RG flow equations

$$\frac{d\nu_2}{d\ell}=(z-2)\nu_2+K_d\frac{d+2}{d}\frac{\lambda_{13}D\Lambda^d}{\nu}, \tag{A28}$$

$$\frac{d\nu_4}{d\ell}=(z-4)\nu_4-\frac{K_d}{d}\frac{\lambda_{22}^2D_s\Lambda^d}{\nu^3}, \tag{A29}$$

which determine the renormalized coefficients $\nu_2(\ell)$ and $\nu_4(\ell)$ under infinitesimal RG transformations. As pointed out in the main text, the correction in Eq. (A29) is different by a factor of 4 from the result reported in Ref. [24] for the case $\nu_2=0$ and $\lambda_{13}=0$, but consistent with Refs. [25,29].

Next, consider the intermediate flow equation for λ_{13} given in Fig. 9, which translates into mathematics as

$$\lambda_{13}^{<} = \lambda_{13} + \sum_{n=1}^{8} \Xi_n = \lambda_{13} - K_d \frac{d^2 + 6d + 20}{d(d+2)} \frac{\lambda_{13}^2 D \Lambda^d}{\nu^2} d\ell, \tag{A30}$$

where we have divided out the external momenta. The renormalized coupling constant $\tilde{\lambda}_{13}$ is therefore given by

$$\begin{aligned}\tilde{\lambda}_{13} &= e^{(z+2\alpha-4)d\ell} \lambda_{13}^{<} \approx [1 + (z - 2\alpha - 4)d\ell] \lambda_{13}^{<} \\ &= [1 + (z + 2\alpha - 4)d\ell] \lambda_{13} \left\{ 1 - K_d \frac{d^2 + 6d + 20}{d(d+2)} \frac{\lambda_{13} D}{\nu^2} d\ell \right\}.\end{aligned} \tag{A31}$$

Thus, taking $d\ell \to 0$ we obtain the flow equation

$$\frac{d\lambda_{13}}{d\ell} = (z - 4 + 2\alpha)\lambda_{13} - K_d \frac{d^2 + 6d + 20}{d(d+2)} \frac{\lambda_{13}^2 D \Lambda^d}{\nu^2}. \tag{A32}$$

Similarly, the intermediate flow equation for λ_{22} given in Fig. 9 is

$$\lambda_{22}^{<} = \lambda_{22} + \sum_{i=1}^{4} \Gamma_n = \lambda_{22} - 2K_d \frac{d+2}{d} \frac{\lambda_{13}\lambda_{22} D \Lambda^d}{\nu^2} d\ell, \tag{A33}$$

where we have divided out the external momenta. The derivation of the RG flow equation for λ_{22} proceeds along analogous steps as for λ_{13}, with the result in Eq. (29).

Finally, the intermediate RG equation for $\mathcal{D}_F$ in Fig. 9 is given by

$$2\mathcal{D}_F^{<}(\mathbf{k}) = 2\mathcal{D}_F(\mathbf{k}) + \Delta = 2\mathcal{D}_F(\mathbf{k}) + 2k^4 K_d \frac{\lambda_{22}^2 D^2 \Lambda^{d-2}}{\nu^3} d\ell. \tag{A34}$$

Substituting into this equation the expressions of $\mathcal{D}_F^{<}$ and $\mathcal{D}_F$ according to Eq. (A9) we thus find

$$D_0^{<} + D_2^{<} k^2 + D_4^{<} k^4 = D_0 + D_2 k^2 + D_4 k^4 + k^4 K_d \frac{\lambda_{22}^2 D^2 \Lambda^{d-2}}{\nu^3} d\ell, \tag{A35}$$

from which it is clear that to one-loop order only D_4 is being renormalized. Indeed, if D_4 had not been included in the original expression for $\mathcal{D}_F$, it would have been generated under the RG; i.e., even if $D_4=0$ for $\ell=0$, D_4 becomes finite for $\ell>0$. Although D_4 is a higher-order term in k relative to D_0 and D_2, we nevertheless include this term [25] because it represents the leading-order correction to the noise covariance. The derivation of the RG flow equations for D_0, D_2, and D_4 follows the same steps as for the propagator and results in Eqs. (30)–(32).

APPENDIX B: LOCATION OF FIXED POINTS

The general expressions for the EW fixed point, the MH fixed point, and FP1 can be found in Table I. In this appendix we compile expressions for the remaining fixed points of Eqs. (43)–(47) for any substrate dimensions d. A detailed calculation of these fixed points can be found in Ref. [50]. FP2 is given by

$$r = \frac{(1-B)d}{d-4B}, \quad u_1 = \frac{4-d}{d-4B}, \quad u_2 = 0, \quad \Gamma_2 = 0, \quad \Gamma_4 = 0. \tag{B1}$$

The VLDS$^{\pm}$ fixed point is

$$r = 1, \quad u_1 = 0, \quad u_2^2 = \frac{4-d}{6C[6 - d + \Gamma_4(2-d)]}, \quad \Gamma_2 = 0,$$

$$\Gamma_4 = \frac{1}{2a_1}\{-b_1 \pm \sqrt{48[a_1 + b_1 + c_1 + 3(2-d)^2]}\}, \tag{B2}$$

in which a_1, b_1, and c_1 are

$$a_1 = 12(2-d) - d(4-d), \quad b_1 = 48 + 12(2-d) - 2d(4-d),$$

$$c_1 = -d(4-d). \tag{B3}$$

Finally, FP3$^{\pm}$ is located at

$$r = \frac{d(d - 14B + 2)}{d(2+d) - 4B(2+3d)}, \tag{B4}$$

$$u_1 = \frac{4-d}{(3d - 28B)(1 + \Gamma_4)}, \tag{B5}$$

$$u_2^2 = \frac{d(d-4)[168B^2 + d(2+d) - 2B(12+13d)]}{2C(28B-3d)[-d(2+d)(-6+d-2\Gamma_4+d\Gamma_4) + 4B\{-8 + 3d^2(1+\Gamma_4) - d(17+5\Gamma_4)\}]}, \tag{B6}$$

$$\Gamma_2 = 0, \tag{B7}$$

$$\Gamma_4 = \frac{1}{2a_2}(-b_2 \pm \sqrt{b_2^2 - 4a_2c_2}), \tag{B8}$$

where a_2, b_2, and c_2 are

$$a_2 = Cd[-56B^2(40 - 36d + 3d^2) - d(48 - 8d - 14d^2 + d^3) + 2B(224 + 72d - 168d^2 + 13d^3)], \tag{B9}$$

$$b_2 = -2C[d^2(72 + 16d - 8d^2 + d^3) + 56B^2(32 + 68d - 24d^2 + 3d^3) - 2Bd(432 + 268d - 104d^2 + 13d^3)], \tag{B10}$$

$$c_2 = -C(d-4)d^2[168B^2 + d(2+d) - 2B(12 + 13d)]. \tag{B11}$$

[1] A.-L. Barabási and H. E. Stanley, *Fractal Concepts in Surface Growth* (Cambridge University Press, Cambridge, England, 1995).
[2] T. Halpin-Healy and Y.-C. Zhang, Phys. Rep. **254**, 215 (1995).
[3] T. Toffoli and N. Margolus, *Cellular Automata Machines* (MIT Press, Cambridge, MA, 1987).
[4] D. H. Rothman and S. Zaleski, *Lattice-Gas Cellular Automata: Simple Models of Complex Hydrodynamics* (Cambridge University Press, Cambridge, England, 1997).
[5] B. Chopard and M. Droz, *Cellular Automata Modeling of Physical Systems* (Cambridge University Press, Cambridge, England, 1998).
[6] D. D. Vvedensky, J. Phys.: Condens. Matter **16**, R1537 (2004).
[7] *Theory and Applications of Cellular Automata*, edited by S. Wolfram (World Scientific, Singapore, 1986).
[8] *Lattice Gas: Theory Application, and Hardware*, edited by G. D. Doolen (MIT Press, Cambridge, MA, 1991).
[9] N. Gershenfeld, *The Nature of Mathematical Modelling* (Cambridge University Press, New York, 1999), Chap. 9.
[10] T. Liggett, *Stochastic Interacting Systems: Contact, Voter, and Exclusion Processes* (Springer-Verlag, New York, 1999).
[11] B. A. Joyce, Rep. Prog. Phys. **48**, 1637 (1985).
[12] J. Y. Tsao, *Materials Fundamentals of Molecular Beam Epitaxy* (Academic, Boston, 1993).
[13] M. A. Herman and H. Sitter, *Molecular Beam Epitaxy: Fundamentals and Current Status*, 2nd ed. (Springer-Verlag, Berlin, 1996).
[14] A. Pimpinelli and J. Villain, *Physics of Crystal Growth* (Cambridge University Press, Cambridge, England, 1999).
[15] I. V. Markov, *Crystal Growth for Beginners: Fundamentals of Nucleation, Crystal Growth and Epitaxy*, 2nd ed. (World Scientific, Singapore, 2003).
[16] T. Michely and J. Krug, *Islands, Mounds, and Atoms: Patterns and Processes in Crystal Growth far from Equilibrium* (Springer-Verlag, New York, 2004).
[17] P. Kratzer and M. Scheffler, Phys. Rev. Lett. **88**, 036102 (2002).
[18] M. Basham, P. A. Mulheran, and F. Montalenti, Surf. Sci. **565**, 289 (2004).
[19] A. F. Voter, in *Radiation Effects in Solids*, Proceedings of the NATO Advanced Study Institute on Radiation Effects in Solids, edited by K. E. Sickafus, E. A. Kotomin, and B. P. Uberuaga (Springer-Verlag, Berlin, 2007).
[20] T. Shitara, D. D. Vvedensky, M. R. Wilby, J. Zhang, J. H. Neave, and B. A. Joyce, Phys. Rev. B **46**, 6815 (1992).
[21] T. Shitara, D. D. Vvedensky, M. R. Wilby, J. Zhang, J. H. Neave, and B. A. Joyce, Phys. Rev. B **46**, 6825 (1992).
[22] M. Kardar, G. Parisi, and Y.-C. Zhang, Phys. Rev. Lett. **56**, 889 (1986).
[23] E. Medina, T. Hwa, M. Kardar, and Y.-C. Zhang, Phys. Rev. A **39**, 3053 (1989).
[24] Z.-W. Lai and S. Das Sarma, Phys. Rev. Lett. **66**, 2348 (1991).
[25] L.-H. Tang and T. Nattermann, Phys. Rev. Lett. **66**, 2899 (1991).
[26] C. Herring, in *The Physics of Powder Metallurgy*, edited by W. E. Kingston (McGraw-Hill, New York, 1951), pp. 143–179.
[27] W. W. Mullins, J. Appl. Phys. **28**, 333 (1957).
[28] S. F. Edwards and D. R. Wilkinson, Proc. R. Soc. London, Ser. A **381**, 17 (1982).
[29] T. Sun, H. Guo, and M. Grant, Phys. Rev. A **40**, 6763(R) (1989).
[30] J. Villain, J. Phys. I **1**, 19 (1991).
[31] M. D. Johnson, C. Orme, A. W. Hunt, D. Graff, J. Sudijono, L. M. Sander, and B. G. Orr, Phys. Rev. Lett. **72**, 116 (1994).
[32] K. A. Bratland, Y. L. Foo, J. A. N. T. Soares, T. Spila, P. Desjardins, and J. E. Greene, Phys. Rev. B **67**, 125322 (2003).
[33] F. Buatier de Mongeot, W. Zhu, A. Molle, R. Buzio, C. Boragno, U. Valbusa, E. G. Wang, and Z. Zhang, Phys. Rev. Lett. **91**, 016102 (2003).
[34] H.-C. Kan, S. Shah, T. T. Tadayyon-Eslami, and R. J. Phaneuf, Phys. Rev. Lett. **92**, 146101 (2004).
[35] H.-C. Kan, R. Ankam, S. Shah, K. M. Micholsky, T. Tadayyon-Eslami, L. Calhoun, and R. J. Phaneuf, Phys. Rev. B **73**, 195410 (2006).
[36] T. Tadayyon-Eslami, H.-C. Kan, L. C. Calhoun, and R. J. Phaneuf, Phys. Rev. Lett. **97**, 126101 (2006).
[37] S. Pal, D. P. Landau, and K. Binder, Phys. Rev. E **68**, 021601 (2003).
[38] S. Das Sarma, P. P. Chatraphorn, and Z. Toroczkai, Phys. Rev. E **65**, 036144 (2002).
[39] W. Zhu, F. B. de Mongeot, U. Valbusa, E. G. Wang, and Z. Zhang, Phys. Rev. Lett. **92**, 106102 (2004).
[40] A. Ballestad, B. J. Ruck, M. Adamcyk, T. Pinnington, and T. Tiedje, Phys. Rev. Lett. **86**, 2377 (2001).
[41] A. Ballestad, B. J. Ruck, J. H. Schmid, M. Adamcyk, E. Nodwell, C. Nicoll, and T. Tiedje, Phys. Rev. B **65**, 205302 (2002).
[42] D. D. Vvedensky, A. Zangwill, C. N. Luse, and M. R. Wilby, Phys. Rev. E **48**, 852 (1993).
[43] M. Předota and M. Kotrla, Phys. Rev. E **54**, 3933 (1996).
[44] G. Costanza, Phys. Rev. E **55**, 6501 (1997).
[45] C. A. Haselwandter and D. D. Vvedensky, Phys. Rev. Lett. **98**, 046102 (2007).
[46] C. A. Haselwandter and D. D. Vvedensky, Europhys. Lett. **77**, 38004 (2007).

[47] C. A. Haselwandter and D. D. Vvedensky (unpublished).
[48] C. Baggio, R. Vardavas, and D. D. Vvedensky, Phys. Rev. E **64**, 045103(R) (2001).
[49] Alvin L.-S. Chua, C. A. Haselwandter, C. Baggio, and D. D. Vvedensky, Phys. Rev. E **72**, 051103(R) (2005).
[50] C. A. Haselwandter, Ph.D. thesis, University of London, 2007 (unpublished). Available online at http://www.imperial.ac.uk/research/cmth/research/theses/.
[51] D. E. Wolf and J. Villain, Europhys. Lett. **13**, 389 (1990).
[52] S. Clarke and D. D. Vvedensky, Phys. Rev. B **37**, 6559 (1988).
[53] P. Šmilauer and M. Kotrla, Phys. Rev. B **49**, 5769 (1994).
[54] M. Kotrla and P. Šmilauer, Phys. Rev. B **53**, 13777 (1996).
[55] N. G. van Kampen, *Stochastic Processes in Physics and Chemistry*, 2nd ed. (North-Holland, Amsterdam, 1992).
[56] C. Haselwandter and D. D. Vvedensky, J. Phys. A **35**, L579 (2002).
[57] C. A. Haselwandter and D. D. Vvedensky, in *Modeling of Morphological Evolution at Surfaces and Interfaces*, edited by J. Evans, C. Orme, M. Asta, and Z. Zhang Mater. Res. Soc. Symp. Proc. Vol. 859E (Materials Research Society, Pittsburgh, 2005), pp. JJ8.8.1–JJ8.8.6.
[58] M. C. Bartelt and J. W. Evans, Phys. Rev. B **46**, 12675 (1992).
[59] J. W. Evans and M. C. Bartelt, Phys. Rev. E **49**, 1061 (1994).
[60] T. G. Kurtz, J. Appl. Probab. **8**, 344 (1971).
[61] T. G. Kurtz, J. Chem. Phys. **57**, 2976 (1972).
[62] T. G. Kurtz, Math. Prog. Stud. **5**, 67 (1976).
[63] T. G. Kurtz, Stochastic Proc. Appl. **6**, 223 (1978).
[64] W. Horsthemke and L. Brenig, Z. Phys. B **27**, 341 (1977).
[65] W. Horsthemke, M. Malek-Mansour, and L. Brenig, Z. Phys. B **28**, 135 (1977).
[66] P. Hänggi, Z. Phys. B **30**, 85 (1978).
[67] R. F. Fox and J. Keizer, Phys. Rev. A **43**, 1709 (1991).
[68] Comment by W. Horsthemke following the talk by R. Graham, in *Order and Fluctuations in Equilibrium and Nonequilibrium Statistical Mechanics*, Proceedings of the XVIIth International Solvay Conference on Physics, edited by G. Nicolis, G. Dewel, and J. W. Turner (Wiley, New York, 1981), pp. 282–286.
[69] A. R. Bulsara and W. C. Schieve, Phys. Rev. A **18**, 2253 (1978).
[70] L. Vicente, R. F. Rodriguez, and F. Soto, J. Phys. A **19**, 2715 (1986).
[71] C. A. Haselwandter and D. D. Vvedensky, Phys. Rev. E **73**, 040101(R) (2006).
[72] C. A. Haselwandter and D. D. Vvedensky, Phys. Rev. B **74**, 121408(R) (2006).
[73] O. Pierre-Louis, C. Misbah, Y. Saito, J. Krug, and P. Politi, Phys. Rev. Lett. **80**, 4221 (1998).
[74] S. Das Sarma and R. Kotlyar, Phys. Rev. E **50**, R4275 (1994).
[75] M. R. Wilby, D. D. Vvedensky, and A. Zangwill, Phys. Rev. B **46**, 12896(R) (1992).
[76] J. M. López, M. Castro, and R. Gallego, Phys. Rev. Lett. **94**, 166103 (2005).
[77] S.-K. Ma and G. F. Mazenko, Phys. Rev. B **11**, 4077 (1975).
[78] S.-K. Ma, *Modern Theory of Critical Phenomena* (Benjamin/Cummings, Reading, MA, 1976).
[79] P. C. Hohenberg and B. I. Halperin, Rev. Mod. Phys. **49**, 435 (1977).
[80] D. Forster, D. R. Nelson, and M. J. Stephen, Phys. Rev. A **16**, 732 (1977).
[81] T. S. Chang, D. D. Vvedensky, and J. F. Nicoll, Phys. Rep. **217**, 281 (1992).
[82] J. F. Nicoll, T. S. Chang, and H. E. Stanley, Phys. Rev. Lett. **32**, 1446 (1974).
[83] J. F. Nicoll, T. S. Chang, and H. E. Stanley, Phys. Rev. B **12**, 458 (1975).
[84] J. F. Nicoll and T. S. Chang, Phys. Rev. B **18**, 6324 (1978).
[85] J. F. Nicoll, T. S. Chang, and H. E. Stanley, Phys. Rev. A **13**, 1251 (1976).
[86] S-C. Park and J.-M. Park, Phys. Rev. E **67**, 010103(R) (2003).
[87] A. Lazarides, Phys. Rev. E **73**, 041605 (2006).
[88] A possible reason for the discrepancy is that different notations are used in Refs. [24] and [25,29]—the coefficients of the vertices differ by a factor of 1/2. So a superficial comparison would suggest that Refs. [24] and [25,29] are consistent. Note, however, that the scaling exponents found in Refs. [24] and [25,29] are independent of Eq. (8a) [24], Eq. (3) [29], and Eq. (12a) [25], and, hence, the central conclusions of neither article are affected by this discrepancy.
[89] W. E. Boyce and R. C. DiPrima, *Elementary Differential Equations*, 5th ed. (Addison-Wesley, New York, 1992), Chap. 9.
[90] These basic steps are described in detail on p. 4087 of Ref. [77].
[91] From the definition of G in Eq. (A6) it might appear that the nonlinear terms should be included in Eq. (A7). However, the graphs contributing to the effective nonlinearity "feed into" G through the RG flow equations. Viewed in terms of ordinary perturbation theory, the effective propagator G can be interpreted as the "deterministic" contribution to the solution u assuming that the nonlinearities are small.
[92] J. Aarts, W. M. Gerits, and P. K. Larsen, Appl. Phys. Lett. **48**, 931 (1986).
[93] W. F. Egelhoff, Jr. and I. Jacob, Phys. Rev. Lett. **62**, 921 (1989).
[94] S. C. Wang and G. Ehrlich, Phys. Rev. Lett. **71**, 4174 (1993).
[95] G. L. Kellogg, Phys. Rev. Lett. **76**, 98 (1996).
[96] Z. Zhang and H. Metiu, Surf. Sci. **245**, 353 (1991).
[97] C. M. Gilmore and J. A. Sprague, Phys. Rev. B **44**, 8950 (1991).
[98] J. W. Evans, D. E. Sanders, P. A. Thiel, and A. E. DePristo, Phys. Rev. B **41**, 5410 (1990).
[99] D. D. Vvedensky, Phys. Rev. E **68**, 010601(R) (2003).
[100] Computer code MATHEMATICA, Wolfram Research, Inc., Urbana-Champaign, IL, version 5.0.
[101] With the approach used here, the number of increments $\Delta\ell$ cannot be related in a quantitative way to the simulation time τ because z varies during crossover regimes.
[102] S. Curtarolo and G. Ceder, Phys. Rev. Lett. **88**, 255504 (2002).
[103] E. B. Tadmor, M. Ortiz, and R. Phillips, Philos. Mag. A **73**, 1529 (1996).
[104] H. J. Jensen, *Self-Organized Criticality: Emergent Complex Behavior in Physical and Biological Systems* (Cambridge University Press, Cambridge, England, 2000).
[105] T. Hwa and M. Kardar, Phys. Rev. A **45**, 7002 (1992).
[106] A. Vespignani, R. Dickman, M. A. Muñoz, and S. Zapperi, Phys. Rev. E **62**, 4564 (2000).
[107] E. T. Lu, Phys. Rev. Lett. **74**, 2511 (1995).
[108] G. Pruessner, Phys. Rev. E **67**, 030301(R) (2003).